hochschule mannheim

MAX PLANCK INSTITUTE
FOR POLYMER RESEARCH

Physical and chemical effects on the dissipation mechanisms of Polydimethylsiloxane elastomers

Master Thesis

Anna Eimer

March 2022

Working Group Prof. Dr. Hans-Jürgen Butt

Max-Planck-Institute for Polymer Research, Main

Supervisor: Prof. Dr. Georg Schied

Second Supervisor: Prof. Dr. Doris Vollmer

Table of contents

Abbreviation Index

GPC	Gel permeation chromatography
LSCM	Laser scanning confocal microscopy
NMR	Nuclear magnetic resonance
PDMS	Polydimethylsiloxane
Pt	Platinum
Wt %	Weight percentage

Figure Index

Table index

Abstract

Elastomers, such as polydimethylsiloxane (PDMS), can hold a great variety of properties and thus are used in a broad range of areas including microfluidics and biomedicine. One challenge that comes along with biomedical devices based on PDMS, like urinary catheters, is bacterial contamination on the PDMS surface, which leads to a high risk of infection. Until now, these infections have been treated surgically by removing the catheter. In order to reduce bacterial adherence, the adhesion force was investigated on a model system between PDMS surfaces and droplets.

To shed light on the capillary interactions between PDMS surfaces and droplets, physical and chemical influences on PDMS surfaces were investigated. The analysis of the surfaces was performed by optical visualization of the wetting ridge with laser scanning confocal microscopy (LSCM). Moreover, the steady-state friction force was monitored utilizing a sensory setup, which is coupled to the LSCM.

Results show that the share of crosslinkers and the addition of oligomers affect the steady-state friction force and the evolution of wetting ridges. Furthermore, the opening year of the used chemicals influences the resulting steady-state friction force.

The data shown here provides a promising foundation for a systematic study to explore the role of elastic PDMS surface on bacterial contamination.

1 Introduction

Elastomers have unique properties such as non-toxicity, high thermal stability, good transparency, chemical inertness, biocompatibility, viscoelasticity, and simple production.[1] These make them suitable for a variety of applications like biocatalytic coatings[2], anticorrosive coatings[3], stretchable wearable electronics[4], microfluidic devices[5], cell culture substrate[1], and medical devices[6].

One important field in which elastomers, such as polydimethylsiloxane (PDMS), are used is biomedicine and biomedical devices, e.g. urinary catheters.[7] However, the main challenge is the susceptibility of PDMS surfaces to bacterial contaminations, which leads to the formation of biofilms.[6] These biofilms consist of bacteria that colonize and accumulate on the PDMS catheter surface.[8], which causes infections during treatment in hospitals (nosocomial infections). In the ongoing pandemic, nosocomial infections have reached new levels.[9] Treatment of these infections is difficult as biofilms can resist host immune defenses and antimicrobial agents. Therefore, the infections are treated surgically by removing the catheter.[10] A better understanding of the interaction between surface and bacteria is necessary to improve the PDMS surface and avoid biofilm formation.[6,8]

The considered system in this thesis is suited as a model system for the described bacterial contamination, due to interaction between the surface and the bacteria film. It is beyond the scope of this study to examine the efficiency of elastic PDMS surfaces on bacteria contamination.

Elastic PDMS surfaces consist of polymer networks that determine the material properties of the materials. When a compatible fluid is added to the polymer network, the network swells, which leads to a modification of the material properties.[11] Recently, the visualization of the effects of fluids in swollen polymeric networks on the evolution of wetting ridges was investigated.[11] Additionally, previous research has established a method to measure directly the steady-state friction force between a droplet and an elastic PDMS surface.[12] Research to date has not yet determined the physical and chemical effects on the evolution of steady-state friction forces and wetting ridges of elastic PDMS surfaces.

This thesis explores the physical and chemical factors that determine the steady-state friction force between a droplet and an elastic surface during droplet sliding and the formation of wetting ridges.
To investigate this, wetting ridges were studied by optical visualization with laser scanning confocal microscopy (LSCM). The steady-state friction force was monitored utilizing a sensory setup, which is coupled to the LSCM. Results show that the share of crosslinkers and the usage of oligomers influence the steady-state friction force and the evolution of wetting ridges. Furthermore, the used chemicals, especially the opening year of the chemicals play an important role in the analyses outcome.

Chapter 2 covers a literature review that includes explanations of thesis-relevant background knowledge. This is followed by the material and methods section (Chapter 3), in which the used chemicals, the experiments, and the methods are described. Chapter 4 analyses the results of the performed experiments and research by focusing on two key themes: The physical and chemical effects of surface dissipation. Chapter 5 presents a conclusion of the research and an outlook of prospective research in this field.

2 Literature Review

In the following chapter, the theory related to this thesis is described.

2.1 Wetting

Wetting phenomena appear in the contact areas of three distinct phases, of which at least two are fluid (liquid or gas). A typical situation is a liquid wetting a solid surface in a gaseous environment. An example of a wetting phenomenon in daily life is raindrops on a window.[13] Wetting and adhesion of a liquid on a solid surface are important processes in many applications like inkjet printing, coating, pesticide spraying, and anti-biofouling.[6]

Wetting behavior depends on surface properties, the droplet volume, and the force balance between adhesive and cohesive forces, which determine the interaction at the three-phase-contact line. Interactions at the three-phase contact line are determined by capillary forces. The contact angles are defined by the drop and surface properties.[14] Surfaces are hydrophilic if the contact angles are smaller than 90°. On hydrophobic surfaces, the water droplet forms a contact angle larger than 90°.

The contact angle is stated as the angle at which a liquid-gas interface meets with the solid surface. The definition of the contact angle follows by the liquid-gas (Υ_{13}), solid-gas (Υ_{23}), and liquid-solid (Υ_{12}) interfacial tensions (Figure 1a)).

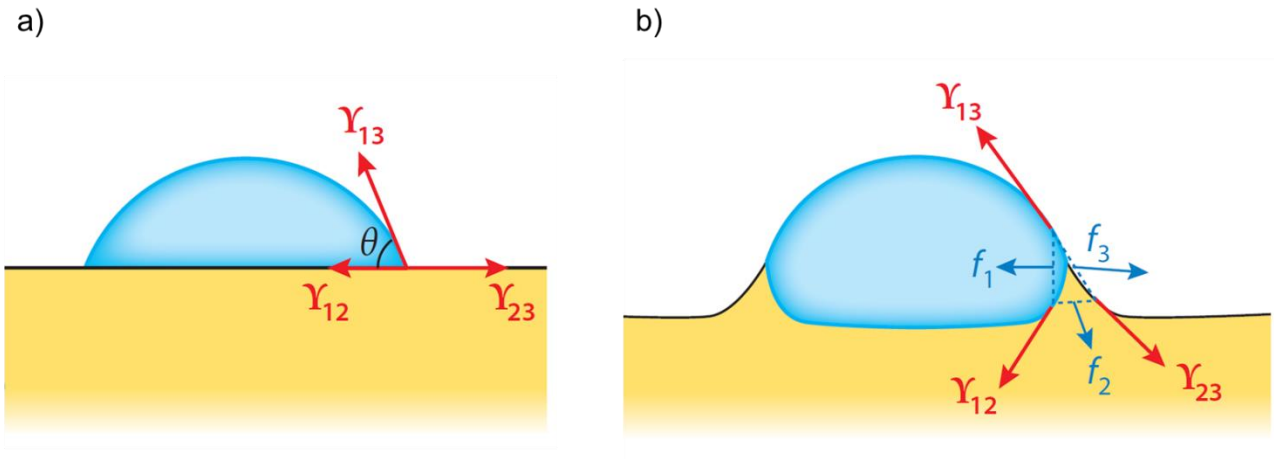

Figure 1: Wetting processes on different surfaces: a) Droplet on a stiff surface. The contact angle θ at the three-phase contact line is defined by the balance of surface tensions. b) Droplet on an elastic surface, the vertical component of the liquid surface tension is balanced by elastic forces in the substrate, resulting in a formation of a wetting ridge at the contact line, from [14].

While the droplet is being in equilibrium, the relation between surface tensions and the contact angle of the liquid at the solid interface is defined by Young's equation[15] :

$$\cos\theta = \frac{\Upsilon_{23} - \Upsilon_{12}}{\Upsilon_{13}} \quad (1)$$

The vertical component of the liquid surface tension (Υ_{13}), points upwards at the three-phase contact line. On elastic solids, this causes a visible deformation - also called wetting ridge - (Figure 1b)), while on stiff solids the deformation does not exist. The shape and size of the wetting ridge are controlled by a balance of surface tension and elastic restoring forces in the bulk of the elastic surface. [11,14]

Young's equation (equation 1) considers chemically homogeneous surfaces. However, surfaces display surface roughness up to micrometer scale, chemical heterogeneities, and solutes. The physical or chemical heterogeneity of real surfaces results in contact angle hysteresis. To evaluate the surface properties, not only the measurement of one contact angle is required, but also the measurement of both the advancing and receding contact angles. The contact angle measured while increasing the droplet volume before the wetting line advances is named the advancing contact angle (θ_{adv}). When liquid volume is removed from the drop and the contact angle is determined before the wetting line recedes, the receding contact angle (θ_{rec}) is measured.[13]

The contact angle hysteresis θ_H is the difference between the advancing and receding contact angle[16] :

$$\theta_H = \theta_{Ad} - \theta_{Re} \quad (2)$$

The contact angle hysteresis represents the homogeneity of surfaces. With a higher value of θ_H the heterogeneity of the surface increases. The consequence of the contact angle hysteresis is friction between droplets and surfaces.[17,18] Friction between droplets and surfaces is discussed in the following section.

2.2 Friction

Friction is the force between surfaces and fluid layers that impedes their relative motion. The friction between a droplet and a surface is driven by adhesion forces. Adhesion forces are induced by strong attraction forces, e.g. van der Waals interactions.[13]

Friction can be differentiated between static and kinetic friction. Static friction must be overcome to initiate motion between a droplet and a surface that is initially stationary. Kinetic adhesion, also called steady-state friction force, is the force between a droplet sliding over surfaces that withstand the motion.[13,17,18]

To describe the force in general, Hooke's law is often used. Hooke's law describes the elastic deformation of solids when their deformation is proportional to the applied stress. The law was published by Robert Hooke in 1678. The law indicates that the deflection x depends linearly on the applied force F and can be formulated[19]:

$$F=k\cdot x \tag{3}$$

K is the spring constant, which characterizes the stiffness of the spring.

Wetting phenomena and the friction forces are influenced by the elastic surface. The behavior of an elastic surface is discussed in the following section.

2.3 Elastic properties

Elastomers consist of polymer networks that have special properties. It exhibits viscous and elastic behavior. Viscous surfaces deform irreversibly by the application of force, while elastic surfaces deform reversibly once the applied force is removed.[20] This response depends on time, temperature, and degree of deformation. The proportion of viscous and elastic behavior of viscoelastic materials depends on the composition of the reactants used.[21]

Elastomers have a very low glass transition temperature. Below this temperature, the polymer networks freeze, leading to embrittlement. The viscoelastic behavior described above is exhibited above the glass transition temperature. The PDMS used in the thesis has a glass transition temperature of -123 °C, which makes it suitable for viscoelastic behavior at room temperature.[22]

Elastomers are typically composed of a polymer (long-chain molecule) and a crosslinker that links the polymer chains. As demonstrated in Figure 2, the distance between the crosslinks (black dots) is larger in Figure 2a) as in Figure 2b), which results in different average mesh sizes. The mesh size influences the material properties, e.g. viscoelasticity of the polymeric network.

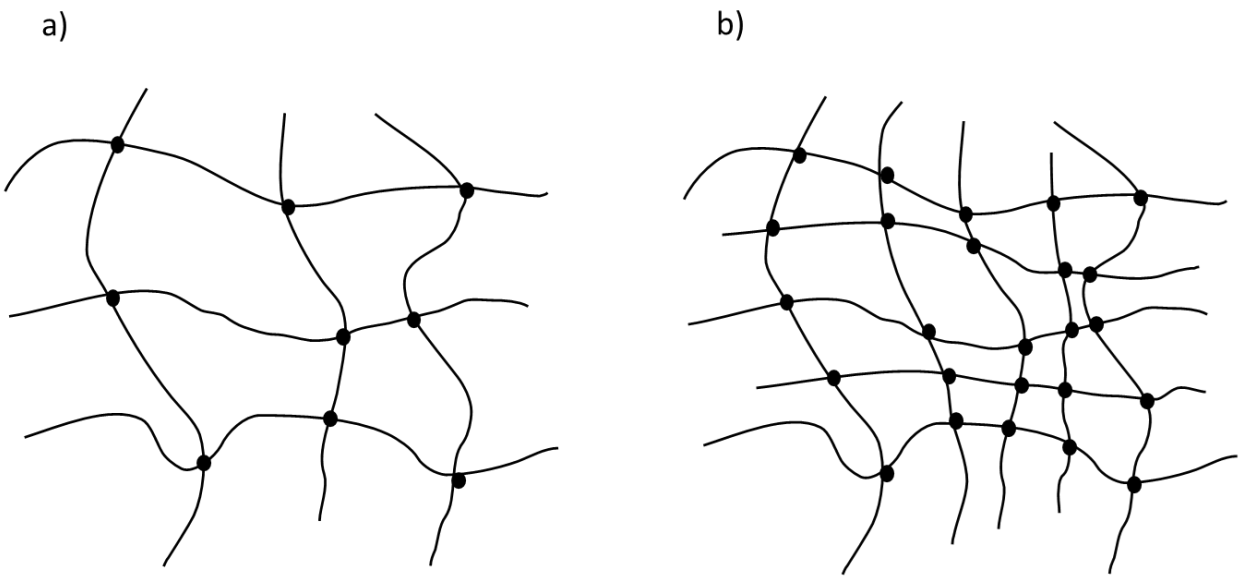

Figure 2: Schema of crosslinked polymer chains (black lines) and crosslinkers (black dots), a) less crosslinked; b) strongly crosslinked.

Polymers are molecules of high molecular mass with a high number of repeating units. In contrast, oligomers are smaller molecules with a minor number of repeating units.[23] Depending on the structure, oligomers can be actively included in the network as crosslinks or copolymers (in this case functional groups are required) or loosely integrated into the network (oligomers without functional groups) (see Figure 3).

Figure 3: Schema of strongly crosslinked polymer chains with added oligomers without functional groups (red lines).

Elastomers can, for example, be composed of silicones. The organosilicon-based polymer PDMS is used in this thesis and is explained in detail in the following section.

2.4 Hydrosilylation reaction

2.4.1 Educts for hydrosilylation reaction

PDMS, an organosilicon-based polymer, is used in many applications e.g. stretchable wearable electronics[4], and urinary catheters[7] due to its chemical inertness, biocompatibility, and viscoelasticity[1].

Sylgard™ 184 elastomer is one of the most frequently used PDMS-based elastomers[24], due to its simple curing and mechanical properties[25].
The ready-made mixture Sylgard™ 184 consists of two parts: a ‘base’ and a ‘crosslinker’, whose chemical compositions are not specified by the company. Analyses do suggest that dimethylvinyl-terminated PDMS (see Figure 4a)) is the main component of the base.[21] The repeating units are composed of a Si-O chain with methyl chains, thus PDMS belongs to the group of organosilicons. The vinyl groups are crucial for the subsequent hydrosilylation reaction. Tetra(trimethylsiloxy)silane structures the polymer network, while dimethylvinylated and trimethylated silica modifies the surface.

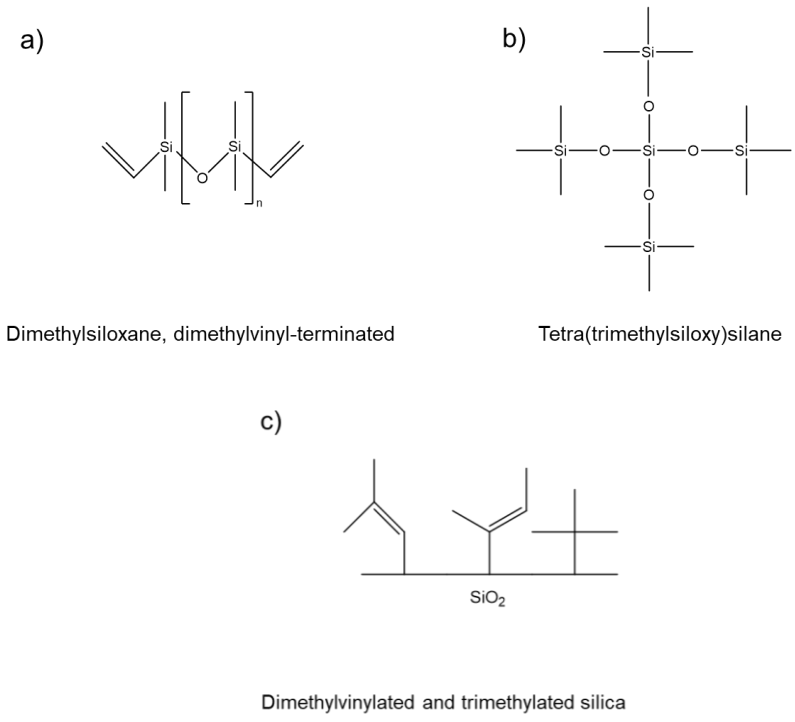

Figure 4: Assumed components of Sylgard™ 184 (‘base’).[21]

For the crosslinker methyl-hydro siloxane-dimethylsiloxane (Figure 5a)) is assumed to be the main component.[21] The hydride bonds play an essential role in the hydrosilylation reaction. It is suspected that the platinum catalyst, which is necessary for the hydrosilylation is present in the crosslinker premix.[26] Tetramethyl tetravinyl cyclotetrasiloxane formats the polymer network, while dimethylvinylated and trimethylated silica modifies the surface.

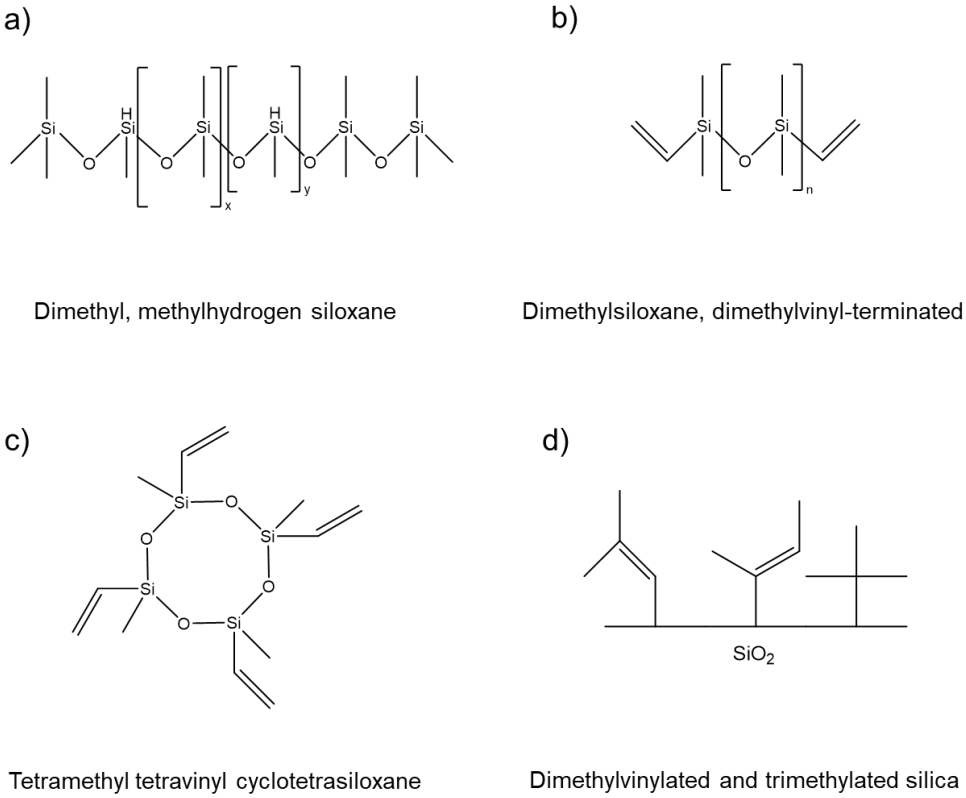

Figure 5: Assumed components of Sylgard™ 184 ('crosslinker')[21].

For the purpose of this thesis, silicone oils such as Octamethyltrisiloxane (Figure 6) are used as oligomers, as their oily consistency allows them to migrate in the polymeric network without crosslinking. In contrast to the vinyl-terminated PDMS used in the base, silicone oil has no functional groups that can react with the crosslinker.

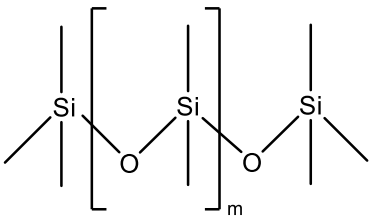

Figure 6: Chemical structure of Octamethyltrisiloxane (oligomer).

2.4.2 Hydrosilylation reaction

The hydrosilylation reaction, which allows the addition of silicon hydride (crosslinker (Figure 5)) across unsaturated double bonds (base (Figure 4)), is a powerful reaction in silicon polymer and surface chemistry.[27]
The reaction (Figure 7) is a syn-selective anti-Markovnikov-addition of a silicone hydride across unsaturated double bonds. Both the base and the crosslinker reveal a Si−O−Si structure with methyl groups and are polymerized through an organometallic cross-linking reaction activated by a Platinum (Pt) based catalyst. As a catalyst, a Pt(0) complex as Karstedt's catalysator might be used for this reaction.[27] New bonds are formed between the vinyl-terminated PDMS group and the hydride group of the crosslinker. The active groups are blue marked, and the newly formed bonds are red marked in Figure 7.

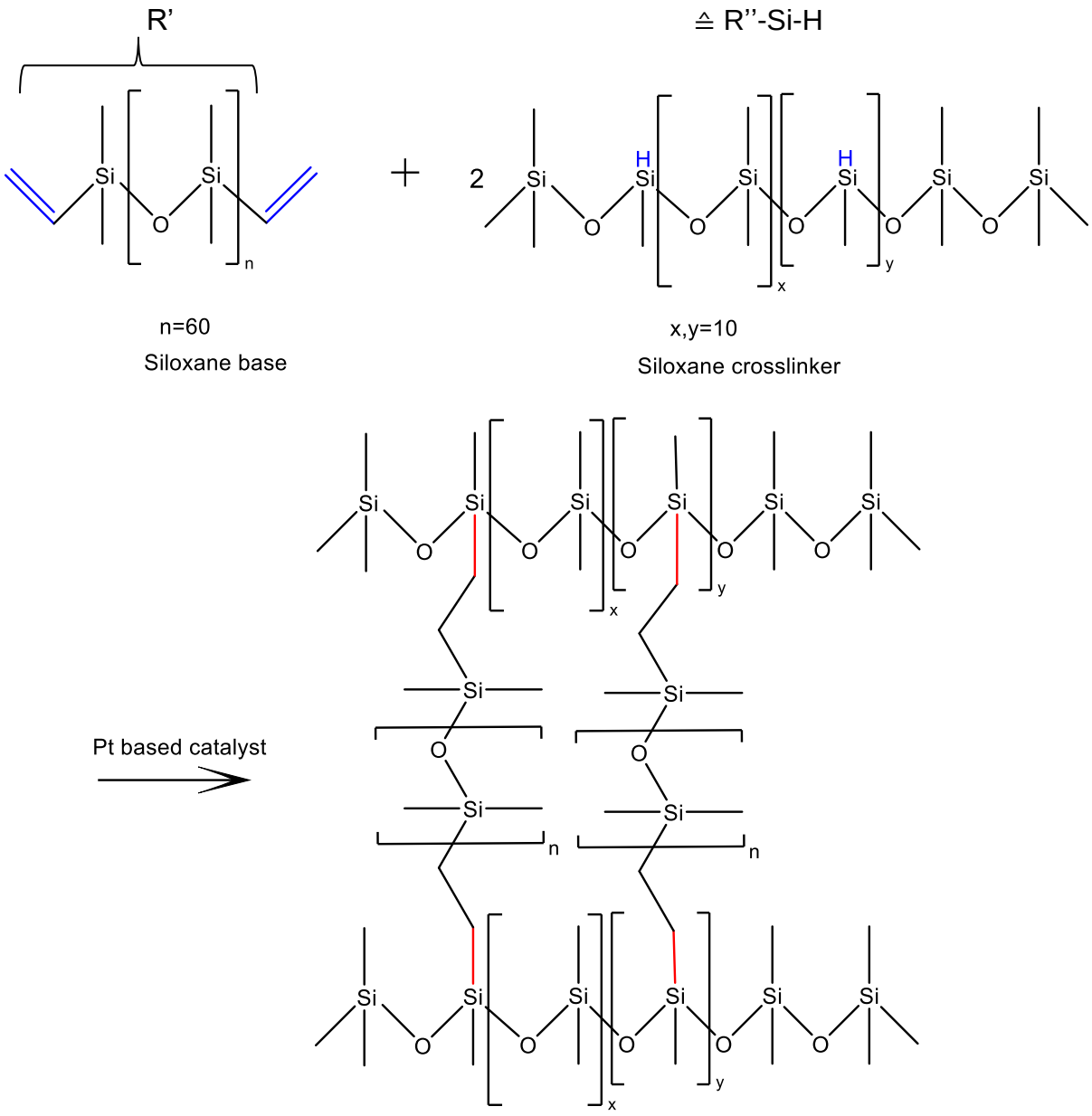

Figure 7: Scheme of hydrosilylation reaction between vinyl-terminated PDMS and methyl-hydro siloxane-dimethylsiloxane crosslinker for silicone elastomers. Crosslinking forms between the vinyl terminated group from the PDMS and the hydride group from the crosslinker in the presence of the Pt-based catalyst. The chemical bonds active in crosslinking are displayed in blue, the red lines show the newly formed crosslinks.

The material properties, such as the viscoelasticity of the produced elastomer, depend on the distance between the crosslinks (see Figure 2).[25] The network structure is determined by the ratio between the educts, the reactivity[28–30] of the functional groups (vinyl and hydride groups) of the educts, and the number of repeating units of the educts, i.e. the molecular weight [31]. The limiting factor of this reaction is the share of crosslinker. The lower the share of crosslinker the greater the number of free polymer chains. Thus, the distance between the crosslinks increases. The higher the share of crosslinkers the smaller the number of free polymer chains, which results in a shorter

distance between the crosslinks. If the functional groups have already reacted with air components before the intended reaction, the reaction can proceed at a lower ratio, which leads to many free chains and more elastic PDMS surfaces. An increasing molecular weight means more repeating units in the polymer chains of the educts, which leads to a larger distance between the crosslinking bonds, resulting in larger average mesh size and more distance between the crosslinks.

These interrelationships become visible through the static visualization of the wetting ridges.[11] There is a presumption that a large distance between the crosslinks causes a higher deformation of the surface, which should be visible as a wetting ridge. It is assumed to make conclusions about the surface properties by sliding a droplet over an elastic PDMS surface (via steady-state friction force). The steady-state friction force might decrease as the distance between the crosslinks increases due to the higher deformation of the elastic PDMS surface.

Figure 8 illustrates the reaction mechanism with R’ being the siloxane chain of the base (see Figure 7 above). For the described reaction the important functional group of the crosslinker is the silicone hydride, therefor the other three residues (two different siloxane chains and the methyl group) are defined as R’’.

2.4.3 Reaction mechanism of platinum-catalyzed hydrosilylation (Chalk-Harrod)

The reaction proceeds according to the mechanism of Chalk-Harrod, illustrated in Figure 8. The mechanism was suggested by Chalk and Harrod in 1965.[32] The siloxane chain of the base is stated as R' (see Figure 7 above the chemical structures). The crosslinker is abbreviated as R’’- Si-H with the residues standing for the two different siloxane residues and the methyl group. These three residues do not influence the newly created bond.

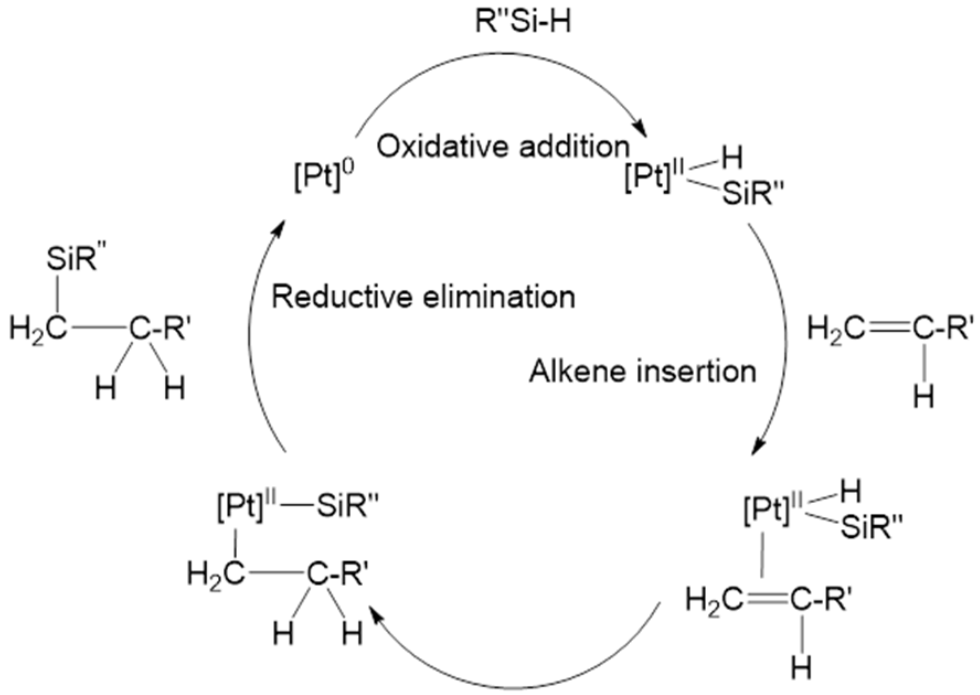

Figure 8: Reaction mechanism of platinum-catalyzed hydrosilylation (Chalk-Harrod).

The mechanism is initiated with a coupled oxidative addition of silane by the Pt(0) complex. Then, the Pt(II) complex coordinates to the alkene group. By adding the SiR'' group a C-H bond and a C-Si bond is formed, while the vinyl bond opens. The product is formed by the reductive elimination of the Pt(II) complex.

2.5 Laser scanning confocal microscopy (LSCM)

LSCM is a combination of fluorescence microscopy and confocal microscopy.[33] In the next section, both microscope techniques are explained.

2.5.1 Fluorescent dyes

For the purpose of this thesis, two organic dyes were chosen such that their fluorescence spectra are sufficiently far separated and a clear distinction between the fluorescent signals is possible (see Figure 9).

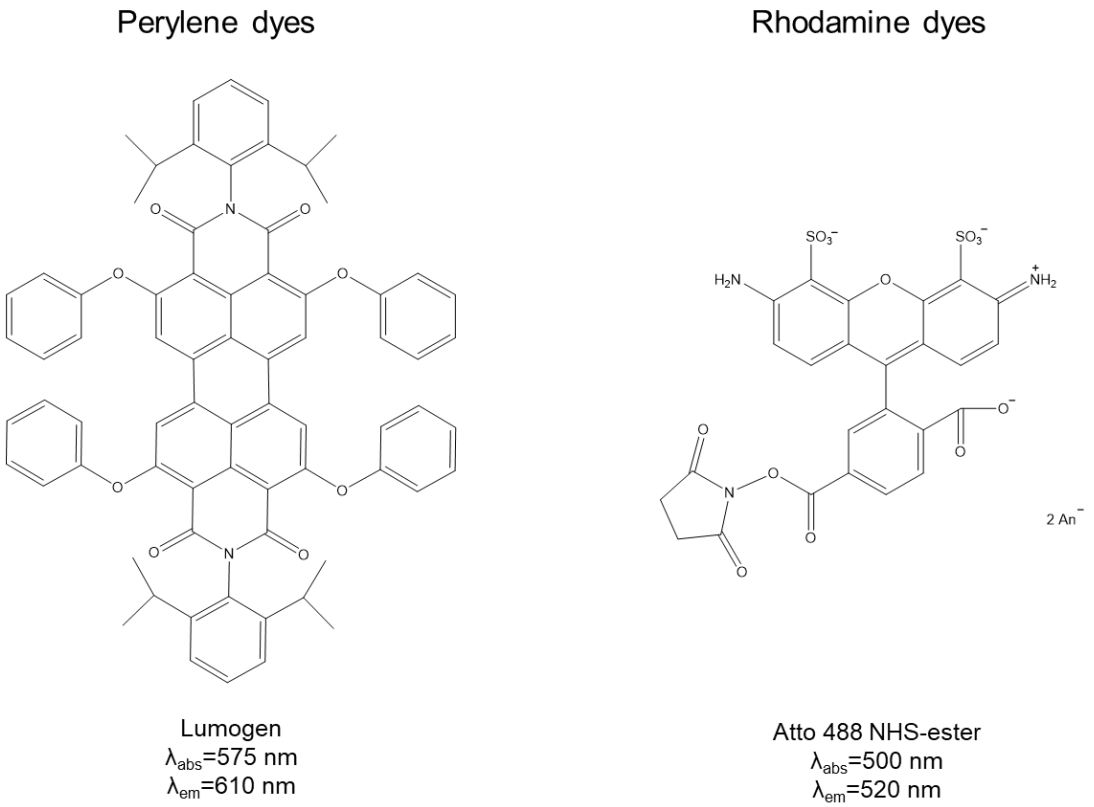

Figure 9: Chemical structure of fluorescent dyes used for LSCM and their absorption maxima (λ_{abs}) and their emission maxima (λ_{em}).

When light irradiates aromatic conjugated molecules (Figure 9), the π-electron systems of these molecules absorb the incident light first. These electrons, therefore, move from the highest occupied energy band (π-band) (S_0) to the lowest unoccupied energy band (π∗-band) (S_1, S_2) of the molecule (Figure 10). The electrons then relax from the lowest energy level of the excited state (S_1) to the ground state (S_0) by emitting certain amounts of energy in the form of light. This emitted light results in fluorescence. The wavelength at which the absorption and emission occurs is given by the bandgap between the highest occupied energy band and the lowest unoccupied energy band. Since electron dynamics is more complex, absorption and emission can be seen over a continuum of energies, resulting in an absorption and emission spectrum rather than a sharp, discrete spectrum.

The Jablonski diagram illustrates the possible transitions of electrons involved in the excitation and relaxation of fluorophores (Figure 10a)).

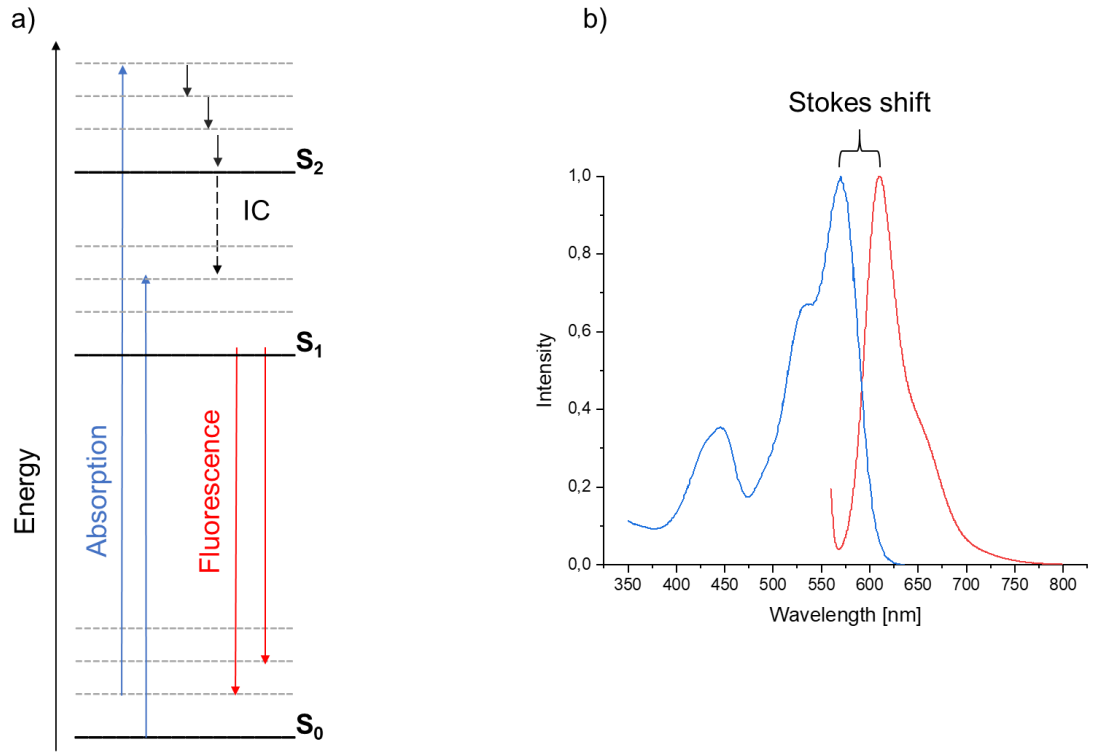

Figure 10: a) Jablonski diagram displaying the excitation of a ground state S_0 to an excited state S_1 through absorption of a photon of energy hv_{abs}, solid arrows depict electronic transitions, curved arrows show vibrational transitions, IC= Internal Conversion; b) Absorption (red line) and emission (blue line) spectra of the fluorophore Lumogen Red F 300 in Polystyrene, data obtained from [34].

Fluorophores are excited in energy levels that are often larger than S_1. As a result of the rapid vibrational relaxation from higher energy levels (dashed arrows in Figure 10a)) to S_1 before emission of the photon, the fluorescence is shifted to longer wavelengths than absorption (Stokes shift, Figure 10b)). This allows separating the two processes spectroscopically.

2.5.2 Fluorescence microscopy

Fluorescence microscopy is an important tool in biological research, as it allows the interaction of certain proteins in cells to be investigated. Only fluorescently labeled regions are imaged, while the rest of the sample is ignored. Figure 11 shows the setup of a fluorescence microscope. The monochromatic excitation light (blue rays) from the laser is reflected by the dichroic mirror. The incident light is bundled by the objective onto the sample (point A). The fluorescent molecules at point A are excited and radiate as fluorescent light (red) in all directions. The emitted light reaches through the objective the dichroic mirror, where the fluorescent light is transmitted. The second objective focuses the light rays and sends them to the detector.

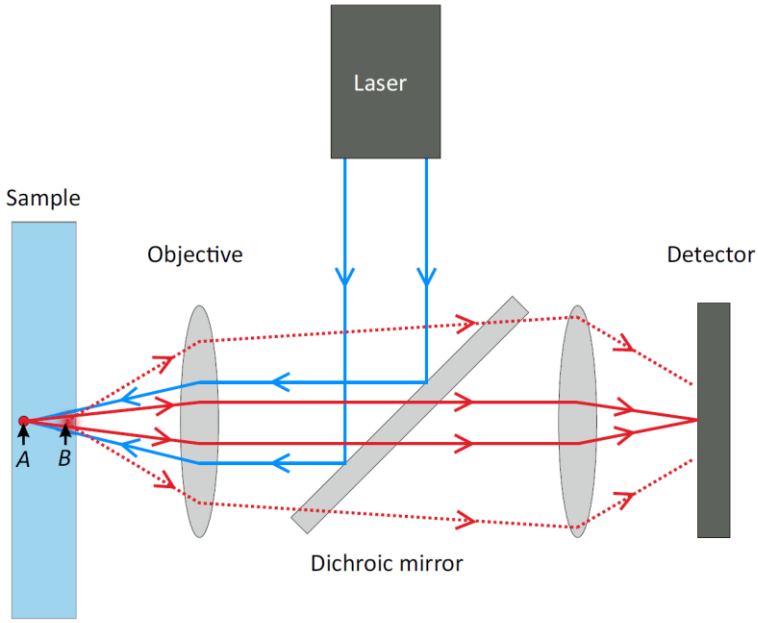

Figure 11: Setup and laser beam of a fluorescent microscope. Point A lies in the focal plane of the lens, and the emitted light from point A reaches the detector. The incident light also illumines areas out-of-focus (e.g. point B), from [35].

The main limitation of fluorescence microscopy, however, is that all fluorescence signals reach the detector and the out-of-focus spots lead to uniform background noise.[33] The incident light also excites the fluorescent molecules at point B in Figure 11. The emitted fluorescent light reaches the detector as an out-of-focus spot. Hence, it is not possible to differentiate the signals in the focal plane from those in the background.

2.5.3 Laser scanning confocal microscopy

In confocal microscopy, the pinhole located at the conjugated plane blocks the out-of-focus light (Point B in Figure 12) to eliminate additional scattered light. The name ‘laser scanning’ comes from the property that the microscope can focus just on one spot, the sample has to be ‘scanned’ with motorized mirrors or stages from spot to spot to image the whole sample.

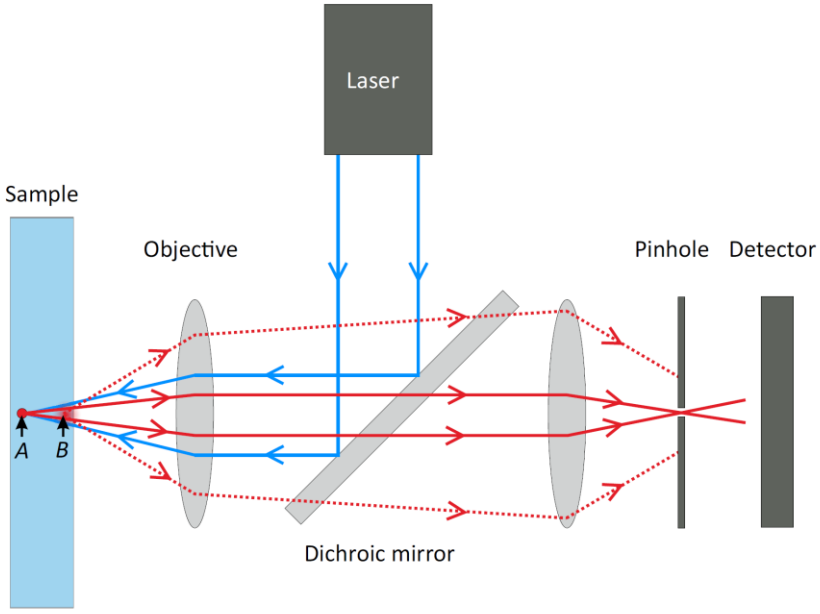

Figure 12: Setup and laser beam of a LSCM. Point A is in the focus of the laser beam and will be detected. The pinhole filters out point B, which is out-of-focus, from [35].

The used LSCM is an inverted microscope. The laser beam crosses the sample from the bottom side. Parts of a sample labeled with different fluorescent dyes can be imaged in reflection mode and various fluorescent modes independently. The emitted fluorescent and reflective signal are captured by a photomultiplier detector. The microscope is also equipped with a piezo objective stage to capture faster cross-sectional images.

3 Materials and methods

In this thesis, wetting properties of elastic PDMS surfaces were analyzed using LSCM in two different modes: determination of steady-state friction force and visualization of the wetting ridge.

In this chapter, the materials and methods are described.

3.1 Chemicals, equipment, and materials

All syntheses were conducted under ambient air and at room temperature. The chemicals were used as supplied. All chemicals are listed in Table 1, the used equipment is depicted in Table 2 and additional materials are shown in Table 3.

Table 1: List of chemicals.

chemical	specification	manufacturer
Acetone	≥ 99,8 %	Honeywell
Atto 488	NHS-Ester	ATTO-TEC
Chloroform	≥ 99,8 %	Fisher Chemical
Ethanol	≥ 99,8 %	Honeywell
Glycerol	≥ 99 %	Sigma Aldrich
Lumogen 300 F Red		BASF
Polystyrene	standard sample	PSS Polymer Standards Service GmbH
Silicone Oil viscosity 50 cSt		Sigma Aldrich
Silicone Oil viscosity 500 cSt		Sigma Aldrich
Sylgard 184 Elastomer Kit		Dow Europe GmbH
Toluene	≥ 99,8 %	Fisher Scientific

Table 2: Equipment.

equipment	manufacturer	description
Accuracy weight	Ohaus	Explorer EX2250 D 22
Plasma oven	Diener	Femto BLS
Sonic Bath	Bandelin electronic	Sonorex RK 52H
Oven	Heraeus	VTr 5022
Confocal microscope	Leica	SP8 TCS
Stir plate	Heidolph	MR 3001K
Gel permeation chromatography (GPC)	Agilent	1260 Infinity II LC
Columns for GPC	PSS Standards Service GmbH	PSS SECcurtiy2,SDV 10^6 A, SDV 10^4 A, and SDV 500 A 300x8mm; 10µm

Table 3: Additional materials.

material	manufacturer	description
Syringe 1 mL	Braun	Injekt- F Luer Solo
High precision microscope cover glasses	Carl Roth	24 x 60 mm, 170 ± 5 µm, Nr. 1,5 H
Vials	Macherey-Nagel GmbH & Co. KG	N24, 40 mL
Screw Caps	Macherey-Nagel GmbH & Co. KG	N24 bonded, closed top
Square Dish	Corning Gosselin SAS	120x15 4 Vents Sterile
Metal Blade		0,13 mm thick, 5 mm wide, 95 mm long
Caliper	MIB-Messzeuge GmbH	0,01 mm
Angle Screwdriver	Format	3 and 5 mm

3.2 Synthesis

The functionalization of the used metal blade and the synthesis of the elastic PDMS surfaces are presented in this section.

3.2.1 Functionalization of the metal blade

To keep the droplet in a balance between elastic PDMS surface and blade, the blade was hydrophobized.

Furthermore, the surface properties (hydrophobicity/hydrophilicity) of the used metal blade influence the drop shape[35], which results in a distinction of the steady-state friction force between the droplet and the PDMS surface. For reliable comparison between the measurements, the blade was functionalized as follows.

The blade was placed in a 40 mL glass vial, containing acetone. The filled vial was put in a sonication bath for 10 minutes. Thereafter, the blade was flushed with nitrogen and dried in an oxygen plasma oven (0.4 mbar) for 10 min. The blade was placed overnight in a 20 ml glass vial filled with silicone oil 500 cSt to achieve a hydrophobic state. On the next day, the blade was cleaned in the sonic bath for 10 min with toluene to remove residual silicone oil. The blade was dried with nitrogen and stored in a sample box. Before measurements, the blade was cleaned with acetone and Milli-Q water.

3.2.2 Synthesis of PDMS surfaces

3.2.2.1 Basic synthesis

To minimize contamination of PDMS surfaces during exposure to ambient air, samples were prepared immediately before use.

As described in 2.4.2 the material properties e.g. viscoelasticity depend on the share of the crosslinker and the number of repeating units of the polymer chains and the molecular weight of the polymer chains, respectively.

To change the material properties, the samples were prepared with different weight ratios of base to crosslinker and additional oligomer (see Table 4). The base, the crosslinker, and Octamethyltrisiloxane (as an oligomer) were mixed in a 40 mL glass vial according to Table 4. The amount of Octamethyltrisiloxane was referred to the amount of the base. The mixture was stirred by hand for 5 min. The viscous mixture was degassed in a vacuum oven (0.5 bar) for 30 min until no air bubbles were observed. Meanwhile, the glass slides were rinsed with ethanol and acetone, dried with nitrogen, and exposed to an oxygen plasma oven (0.4 bar) for 10 min at 300 W to enhance the bond capacity between the hydroxyl groups on the glass slides and the PDMS gel. 1 mL of the mixture was dispensed on the cleaned glass slides. Approximately 100 µm thick PDMS surfaces were created by spin coating at 2000 rpm for 120 s. All samples, if not mentioned differently, were consistently cured in an oven

at 60 °C overnight. After curing, the samples were stored in a covered sample box at room conditions and analyzed three days after synthesis.

A ratio of 10:1 (base to crosslinker) prepared as described above contains 4-5 wt% free chains.[36]

Table 4: Formulation of synthesized surfaces.

Weight Ratio **Base: Crosslinker**	**Octamethyltrisiloxane with a viscosity of 50 cSt**	**Weight Ratio** **Base: Octamethyltrisiloxane**
10:1	-	-
20:1	-	-
30:1	-	-
40:1	-	-
50:1	-	-
60:1	-	-
10:1	+	1:0
10:1	+	1:0.5
10:1	+	1:1
10:1	+	1:1.5

3.2.2.2 Synthesis with chemicals opened in different years

The following experiment aimed to determine the influence of chemicals opened in different years on the steady-state friction force between a droplet and a PDMS surface. The term ‘batch’ defines the elastomer kit opened in a certain year, batch 2016 was opened in 2016. The samples were established as described above. The different combinations of these syntheses are shown in Table 5.

Table 5: Formulation of synthesized surfaces with chemicals from batches opened in different years.

Weight Ratio Base: Crosslinker	Base opened 2021	Crosslinker opened 2021	Base opened 2019	Crosslinker opened 2019	Base opened 2016	Crosslinker opened 2016
10:1	+	+	-	-	-	-
10:1	-	-	+	+	-	-
10:1	-	-	-	-	+	+
10:1	+	-	-	+	-	-
10:1	+	-	-	-	-	+
10:1	-	+	+	-	-	-
10:1	-	+	-	-	+	-

3.2.2.3 Synthesis with different humid surroundings

To analyze the influence of the air humidity, surfaces with the chemical composition of 10:1 (weight ratio of base to crosslinker) were prepared with the chemical batch opened in 2021. Instead of curing in the oven, three samples were dried in a desiccator with low humidity, with nitrogen (around 5 %), and three samples in a desiccator with high humidity with nitrogen and water (around 64 %) for 7 days. Afterward, all samples were dried in an oven under a vacuum overnight and analyzed the next day. The samples were stored in a sample box for four days. After analyzing again from both types (low and high humidity), two samples of each type were put in the desiccators as described. The other samples were stored in a samples box under air conditions. After 7 days/14 days of additional environmental humid influences, the samples from the desiccators were dried in an oven under a vacuum overnight and all samples (also the samples under air conditions) were analyzed the next day.

3.2.3 Synthesis of dyed PDMS surfaces

To minimize contamination of surfaces during exposure to ambient air, samples were prepared immediately before use.

For visualization of the crosslinked network, perylene dye is chemically incorporated into the PDMS network in distinction to [37]. A prepared solution of ~10 mg/mL Lumogen 300 F Red in chloroform was used and stored in a 40 mL glass vial with aluminum foil as sun protection in the laboratory.

The PDMS base and Octamethyltrisiloxane were mixed with mentioned Lumogen–chloroform dispersion (10 mg/mL) in a volume ratio (1:100 mL) in a 40 mL glass vial and stirred with a magnetic stir bar at 300 rpm for 30 min until the mixture was homogeneously mixed. Chloroform solvent was evaporated by placing the base Lumogen 300 F Red mixtures in an oven at 40 °C under vacuum.

The crosslinker was added to the base Lumogen 300 F Red mixture with different weight ratios (see Table 6). Preparation of PDMS coated glass slides followed the same procedure as described in 3.2.2. All samples were consistently cured in an oven at 40 °C overnight. After baking, the samples were stored in a covered sample box and analyzed one week after synthesis.

Table 6: Formulation of synthesized surfaces with Lumogen 300 F Red.

Weight Ratio **Base: Crosslinker**	**Octamethyltrisiloxane with a viscosity of 50 cSt**	**Weight Ratio** **Base: Octamethyltrisiloxane**
10:1	-	-
20:1	-	-
30:1	-	-
40:1	-	-
50:1	-	-
60:1	-	-
10:1	+	1:0
10:1	+	1:0.5
10:1	+	1:1
10:1	+	1:1.5

3.3 Characterization methods

The effects due to different compositions of the PDMS surface will be investigated in this thesis by analyses of the wetting ridge and the steady-state friction force. These characterization methods are presented in the following section.

3.3.1 Laser scanning confocal microscopy

3.3.1.1 Wetting Ridge

Images of wetting ridges were captured on an inverted LSCM equipped with an HC PL APO CS2 63x/1.20 Water objective lens with a correction ring leading to a lateral resolution of 250 nm and an axial resolution of 700 nm.

A prepared droplet liquid, consisting of a mixture of 57% water and 43% glycerol with the rhodamine dye Atto 488, was used. The addition of glycerol reduces evaporation thus keeping the volume constant.
Additionally, a refractive index matching with PDMS makes the height measurements of the wetting ridge more reliable.

Two lasers with wavelengths of 488 nm (Argon laser) and 561 nm (Helium-neon laser) are utilized to excite the Atto 488 dyed droplet and the Lumogen F Red 300 dyed surface separately. These dyes were chosen, such that their fluorescence spectra are sufficiently far separated and a clear distinction between the fluorescent signals is possible, cf. 2.5.1.

A 5 µL glycerol/water droplet was placed on the sample and a cross-sectional image of the surface deformation is taken at a resolution of 512 × 512 pixels in the xz plane with a scanning speed of 600 Hz. The emitted fluorescent signals were simultaneously captured by separate detectors, and a final image showing the signal from each fluorescent dye was constructed.

The images were analyzed by an ImageJ script using thresholding per x line. A baseline correction was done with all images. The images were made binary to identify the surface lines of each phase.

3.3.1.2 Steady-state friction force measurements

The steady-state friction forces were measured with an inverted LSCM using a Leica HC PL APO CS 10x/0.40 dry objective lens by hanging a blade with a stage close to the sample. The blade was positioned such that its free-hanging end hovered some µm above the PDMS sample. The illuminating laser is reflected by the lower edge of the blade. The reflected light is captured and shows the current position of the blade, see Figure 13. By pushing a droplet with a moving sample table against the blade with a force F, the resulting deflection x is given by Hooke's law (see 2.2) where k is the spring constant of the blade. The table moved at a constant speed of 1mm/s over a distance of 1 cm.

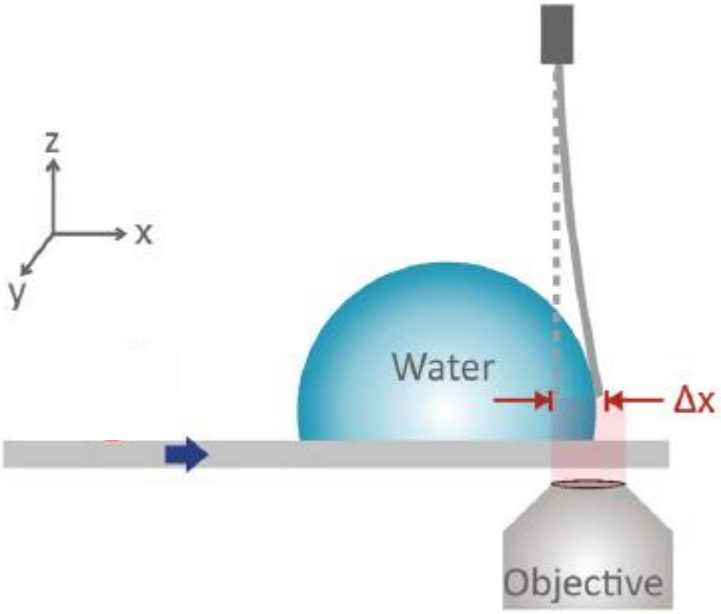

Figure 13: LSCM setup for measuring steady-state friction forces. The surface moves to the right the droplet (blue) butts to the blade (grey), adapted from [12].

The spring constant was quantified for each surface separately by softly deflecting the blade and releasing it, which leads to a damped oscillation over time (see Figure 14) at the blade's resonance frequency.[12] From this oscillation, the spring constant was determined by a Python script, using the mass of the blade, the total length of the blade, and the clamped length of the blade. For calibration of the measured forces the pixel size, and the recording time during calibration and measurement are needed.

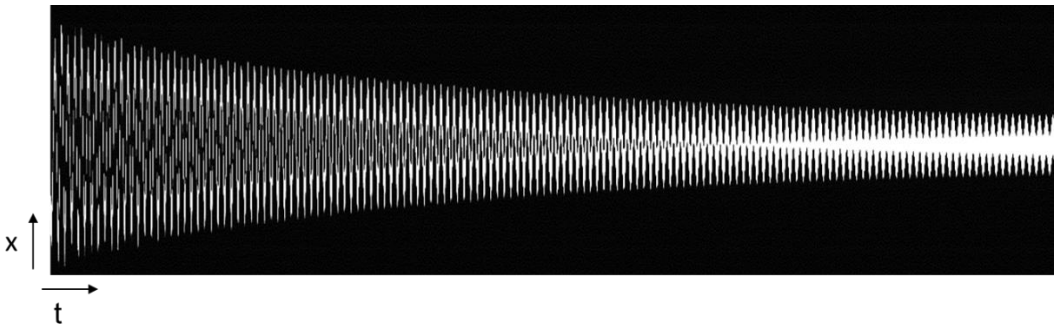

Figure 14: Damped sine oscillation of the blade for determining the spring constant. The x-axis shows the time of the oscillatory motion, the y-axis the intensity of the motion.

Naga et al. [12] published the method to measure the steady-state friction force by sliding a droplet over the surface. In contrast to Naga [35], a mixture of water and glycerol was used as droplet liquid instead of pure water to reduce evaporation. To measure the steady-state friction forces the laser beam was adjusted to the lower-left edge of the blade and a 5 µL dyed Atto 488 dissolved in glycerol/water droplet was deposited onto the surface before the lower right edge of the blade. The displacement of the blade is visible, especially when the laser does not pass through the droplet.

The video was recorded at a resolution of 1024 x 1 pixels with a scanning speed of 400 Hz in xt plane. An Argon laser with a wavelength of 458 nm was used for the recording. The analyses of the forces were done by a Python script using thresholding per x line and center of mass determination. The blade metal dimensions were chosen such that the deflection could be recorded clearly while staying within the maximum measurable range at all times. The time resolution was 1.25 ms.

From each surface, 5 runs were recorded, by using a new droplet each time and a new sliding track on the surface. The videos and images were made binary to identify the blade.

To vary the setup measurements were also done as described above but with a droplet volume of 3 µL or 1 µL, and with a reduced speed of 0.5 mm/s and 0.1 mm/s. Also, it was tried to place the droplet directly behind the blade.

3.3.2 Gel permeation chromatography

The GPC analyses were done to determine the molecular weight of the chemicals opened in different years. Base and crosslinker samples were analyzed by Christine Rosenauer with gel permeation chromatography (GPC) experiments with toluene as eluent. A column set consisting of three columns: SDV 10^6 A, SDV 10^4 A, and SDV 500 A, all of 300 × 8 mm and 10 µm average particle size was used at a flow rate of 1.0 mL/min and a column temperature of 30 °C. The injection volume was 50 µL.

Detection was accomplished with a refractive index detector. Data acquisition and evaluation were performed using WINGPC UniChrom. Calibration was carried out using the universal calibration method with polystyrene standards and the Mark-Houwink coefficients for PDMS in toluene.

3.3.3 Nuclear magnetic resonance spectroscopy

^{1}H-NMR analyses of each initial crosslinker and base were recorded with a 500 MHz NMR spectrometer by Manfred Wagner.

The measurements were done under integrate-able conditions with relaxations delays for the protons of 5 s and silica of 20 s.

The samples were prepared in a glovebox in gas-tight NMR tubes. The spectra were analyzed with TopSpin 3.6.2 Bruker software. The NMR analyses were done to determine and compare the chemical structure and the reactivity of the functional groups of chemicals opened in different years.

4 Results and Discussion

Since the dissipation mechanisms on elastic PDMS surfaces are unclear, the physical and chemical effects were investigated experimentally. In this thesis, steady-state friction force measurements were obtained using a LSCM. These results were completed by wetting ridge analyses, molecular weight distribution study, and reactivity examination. The next chapter describes the results of the current investigation.

4.1 General resulting plots

The next section shows the depiction of the results based on one measurement each for the wetting ridge and the steady-state friction force. The description and analyses of the results follow in 4.2 and 4.3.

4.1.1 Wetting Ridge

Figure 15a) shows a wetting ridge of an elastic PDMS surface with a chemical composition of 60:1 (base to crosslinker). The wetting ridge is well visible between the elastic PDMS surface (marked yellow), droplet (marked blue), and air (black).

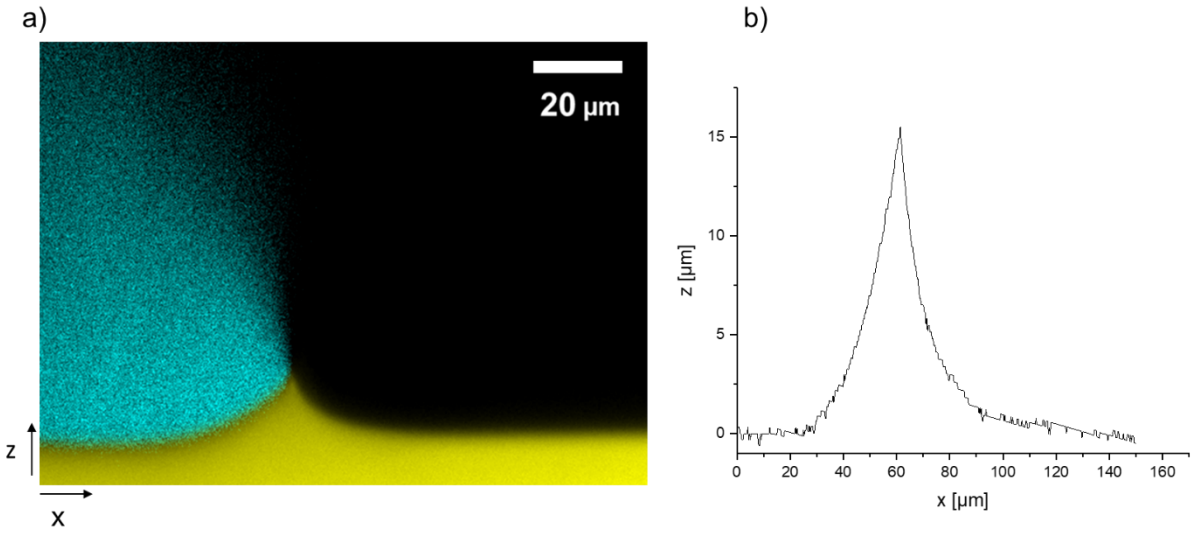

Figure 15: a) Cross-sectional image showing a wetting ridge on a surface with a chemical composition of 60:1 (base to crosslinker). The scale is 20 µm. The yellow part is the PDMS surface, the blue part is the droplet, and the black part is the air; b) Plotted Interface of a).

For quantitative evaluation, a cross-sectional image in the xz-plane was done, see Figure 15a). The interface between the PDMS surface, the droplet, and the air is shown in Figure 15b) exemplary. In the further course, the geometrical analysis of the wetting ridges is done on the interfaces of the wetting ridges as shown in Figure 15b).

4.1.2 Steady-state friction force

As described in 3.3.1.2 the steady-state friction force between the PDMS surface and a droplet was measured with a particular setup. Figure 16a) selected raw data excerpts. The numbers indicate the states, which are denoted in the schematic illustration (Figure 16b)). An exemplary diagram received from the raw data is shown in Figure 16c). The force measurement was done on a PDMS surface with a chemical composition of 10:1 (base to crosslinker). The surface moves over the entire period (see Figure 16b)) to the right at a constant speed (1 mm/s).

Initially, the droplet is located on the surface, in front of the blade (position 0). The surface moves at constant speed towards the blade. This brings the droplet and blade closer to each other (position 1). The ‘snap-in’ is the point, where the blade is drawn to the droplet (position 2) by moving the surface with the droplet to the blade. The snap-in is involved in the hydrophobic blade. The reason for the oscillations during the snap-in is the first venue between droplet and blade. After the snap-in, the moving surface pushes the droplet against the blade, at some point, the droplet slides underneath the blade and positions behind the blade (blue box, position 3-4). The droplet slides in every measurement during the transition state underneath the blade. The reason for this is not clear but it may have to do with the functionalization of the blade.
By pushing the droplet against the blade, the force is increasing till it achieves the maximum (blue box, position 3-4). The largest deformation of the droplet is during the transition state (blue box, position 3-4). The droplet is consecutively dragged along by the blade in a less deformed shape. The droplet sticks to the blade, due to capillary interaction between blade and droplet. This constitutes the transition state (blue box, position 3-4) where the droplet is brought from the static sessile state (position 1) to a kinetic state of steady sliding (red box, position 5).

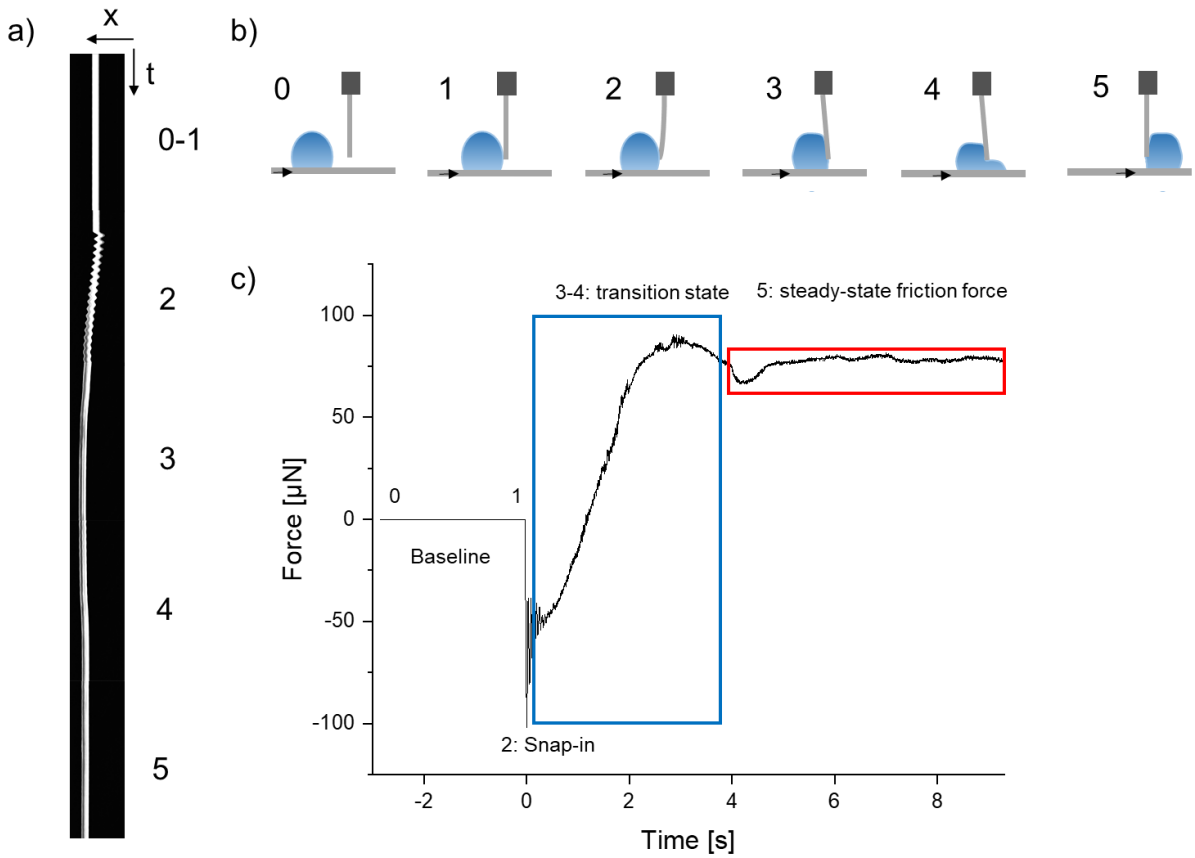

Figure 16: a) Exemplary raw data section, Numbers refer to labeled states in b) and c); b) Schematic illustration moving a droplet and the interaction with the surface; c) Exemplary diagram of a typical force curve received from the raw data (see a)) for a PDMS surface (10:1) (ratio of base to crosslinker)). The x-axis shows the time in s, the y-axis the force in µN.

The steady-state friction force is defined by calculating the average of the steady-state friction force (red box, position 5) for each single force curve. In the following plots (Figure 20, Figure 22, Figure 23, Figure 26, Figure 30), the mean of the average values of 5 runs of the steady-state friction force on one surface is shown.

4.2 Physical effects

For increasing the distance between the crosslinks (see Figure 2) two approaches were tried. In the first approach, the share of the crosslinker in the mixture is reduced, which leads to fewer crosslinking reactions and more unbound polymer chains.
In the second approach, different amounts of Octamethyltrisiloxane as an oligomer are added to the mixture with a defined ratio of base to crosslinker. In this approach the molecular weight of the elastomer increases, which affects the deformation of the surface. The results of these experiments are presented in terms of average steady-state friction force, and wetting ridge.

4.2.1 Change of the crosslinker share

4.2.1.1 Influence on the wetting ridge

The evolution of the wetting ridges on elastic PDMS surfaces with different ratios of the base to crosslinker is presented in Figure 17. The drawn lines are set with offset values to distinguish the lines clearly. The yellow, purple, and green line show a visible wetting ridge on elastic PDMS surfaces with a chemical composition of 60:1 (yellow), 50:1 (purple), and 40:1 (green). The shape and the height of the wetting ridges are dissimilar, the wetting ridge on the surface with a chemical composition of 50:1 of base to crosslinker is significantly wider than the wetting ridges on elastic PDMS surfaces with a chemical composition of 60:1 or 40:1 of base to crosslinker. The height of the wetting ridge of the crosslinked network increases with decreasing share of the crosslinker. The wetting ridges on the elastic PDMS surfaces at a higher crosslinker share depict no visible wetting ridge (see black line (10:1), see red line (20:1), and the blue line (30:1)).

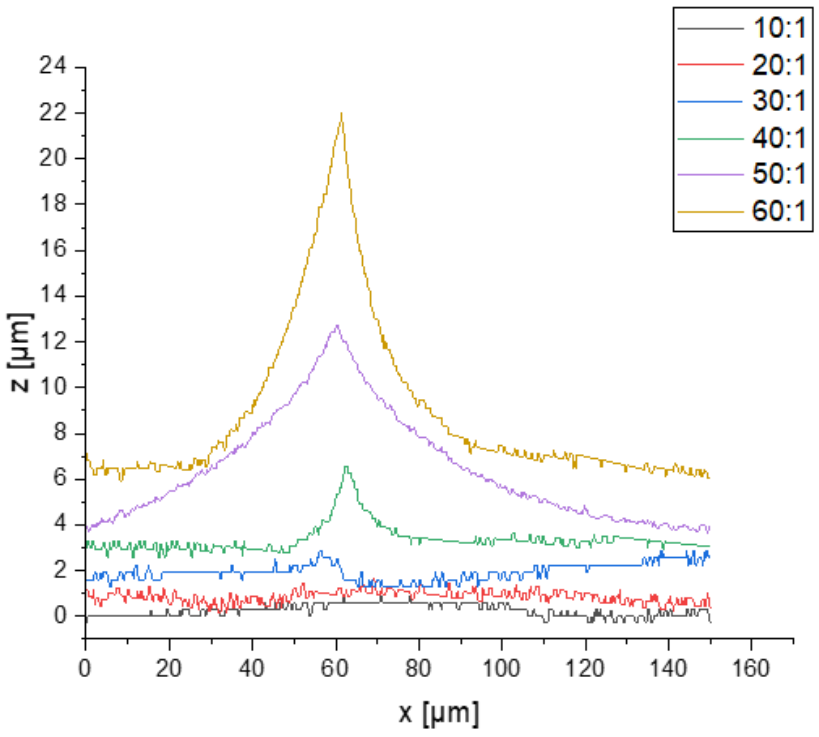

Figure 17: Cross-sectional image showing the evolution of wetting ridges for six elastic PDMS surfaces with a chemical composition of different ratios of base to crosslinker with the droplet on the left side and the air on the right side. The lines are plotted with an offset value to distinguish between the lines. The surface of the grey line has a chemical composition with the highest crosslinker share (ratio of 10:1 (base to crosslinker)), the surface of the red line has a chemical composition with a ratio of 20:1, the surface of the blue line has a chemical composition with a ratio of 30:1, the surface of the green line has a chemical composition with a ratio of 40:1, the surface of the purple line has a chemical composition with a ratio of 50:1, the surface of the yellow line has the lowest crosslinker share (60:1).

These results provide that the share of crosslinkers in the chemical composition of the elastic PDMS surfaces influences the evolution of wetting ridges. It is concluded, that a lower share of crosslinker in the surface leads to a larger wetting ridge, i.e. to a larger deformation. The shape and the size of the wetting ridge indicate that the unbound polymer chains in the surface accumulate at the three-phase contact line.

4.2.1.2 Influence on the steady-state friction force

A curve of a friction force measurement on a surface with a chemical composition of 20:1 (ratio of base to crosslinker) is shown in Figure 18. The measurements were done under the conditions as described in 3.3.1.2 (5 µL volume of the droplet and a constant speed of the sample table of 1 mm/s). The snap-in and the transition state (in which the droplet slides underneath the blade) are observed. However, a steady-state friction force can not be found. The force curve is decreasing rapidly to the baseline around 0 µN. Comparing Figure 16 and Figure 18 shows a clear difference between the elastic PDMS surfaces with a chemical composition of 10:1 and 20:1 (ratio of base to crosslinker).

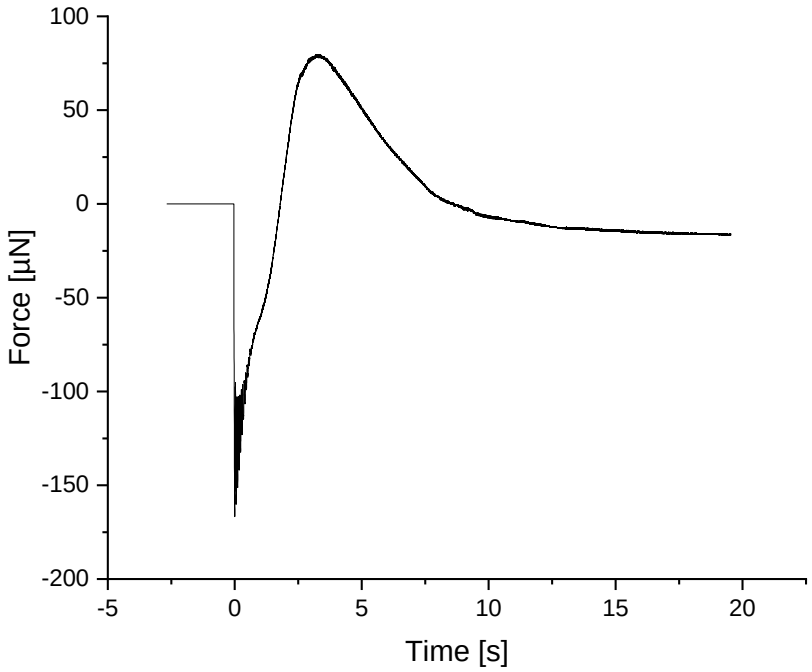

Figure 18: Force measurement curve for an elastic PDMS surface with a chemical composition of 20:1 (base to crosslinker). The x-axis shows the time in s, the y-axis the force in µN.

Figure 18 shows that the procedure sketched in Figure 16b) didn't occur as a negative example. During the measurement, it was observed that the droplet hit the blade, detached from the blade again, and remained on the surface. The results of the elastic PDMS surfaces with a chemical composition of 30:1, 40:1, 50:1, and 60:1 (base to crosslinker) correspond to the curve shown in Figure 18. The droplets remained in all cases on the surface. Furthermore, investigation for reduction of the droplet volume (3 and 1 µL) and a variation of the measurement performance (placing the droplet behind the blade), and a reduction of the constant speed of the sample table (0.5 mm/s and 0.1 mm/s) did not allow a determination of the steady-state friction force.

This finding was unexpected and suggests that the adhesion forces between the droplet and the elastic PDMS surfaces were stronger with less share of crosslinker. This assumption is confirmed by the results of the wetting ridges. The highest wetting ridge is seen on the surface with the lowest amount of crosslinker.

It can thus be suggested that more force is needed to move a droplet on a very elastic surface (less crosslinker share) than on harder surfaces (high crosslinker share). If the movement of the wetting ridge requires more force than capillary forces are applied, the droplet cannot be moved.

These results provide that the ratio of crosslinker influences the seen wetting ridge and the measured steady-state friction force. The steady-state friction force could be just measured for the elastic PDMS surfaces with the highest crosslinker share (60:1), even though the wetting ridge lines between the two smallest ratios (10:1, 20:1, and 30:1) are similar. As described in 2.4.2 the use of a crosslinker is one way, which defines the distance between the crosslinkers in the polymeric PDMS network. Less share of crosslinker means fewer polymer chains can be linked, resulting in loosely connected chains and larger average mesh size and thus a more deformable surface. It is concluded, that the network deformation is greatest with the least crosslinker share. Furthermore, the free polymer chains could accumulate at the three-phase contact line, resulting in the shape and size of the wetting ridge.

4.2.2 Addition of different weight percentages of Octamethyltrisiloxane as an oligomer

4.2.2.1 Influence on the wetting ridge

As discussed in 4.2.1.2 the steady-state friction force could only be measured for the elastic PDMS surfaces with a chemical composition of 10:1 (ratio of base to crosslinker). As follows all elastic PDMS surfaces were synthesized in the mentioned ratio (see Table 4). The evolution of the wetting ridges on elastic PDMS surfaces with a chemical composition of 10:1 is investigated with the addition of different wt % (weight percentage) of Octamethyltrisiloxane in comparison to the base. The results

are presented in Figure 19. The presented lines are set with offset values to distinguish the lines clearly. A clear wetting ridge is seen on the surface with the highest wt % (1.5 wt %) of Octamethyltrisiloxane (green line), whereas a small wetting ridge is visible on the surface with the addition of 1 wt% Octamethyltrisiloxane (blue line). The elastic PDMS surfaces with lower wt % of Octamethyltrisiloxane reveal no observable wetting ridge (red and grey line). The wetting ridge of the crosslinked network increases with the increasing addition of Octamethyltrisiloxane.

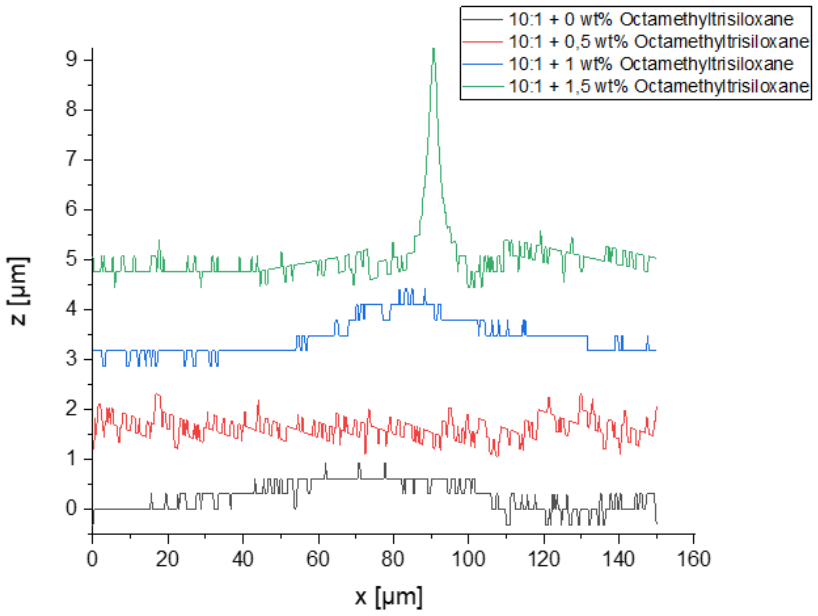

Figure 19: Cross-sectional image showing the evolution of wetting ridges for four elastic PDMS surfaces (10:1) (ratio of base to crosslinker) with the addition of different wt % of Octamethyltrisiloxane in comparison to the base. The lines are plotted with an offset value to distinguish between the lines. The surface without the addition of Octamethyltrisiloxane shows the grey line, the surface with the addition of 0.5 wt % of Octamethyltrisiloxane shows the red line, the surface with the addition of 1 wt % of Octamethyltrisiloxane shows the blue line, the surface with the highest addition of Octamethyltrisiloxane (1.5 wt%) shows the green line.

The admixture of oligomers appears to result in a more deformable surface, which is visible with enough wt % of Octamethyltrisiloxane in a wetting ridge. It is concluded, that the network deformation is greatest with the highest wt % of Octamethyltrisiloxane on the surface. It is possible, that the free oligomer chains accumulate at the three-phase contact line, resulting in the shape and size of the wetting ridge.

4.2.2.2 Influence on the steady-state friction force

The average steady-state friction force values obtained from elastic PDMS surfaces with a chemical composition of 10:1 (ratio of base to crosslinker) with the addition of different wt % of Octamethyltrisiloxane are presented in Figure 20 (see raw data in Appendix Figure 31). For the surface with the chemical composition without Octamethyltrisiloxane, a steady-state friction force of 77 ± 12 µN was measured. With an increasing amount of Octamethyltrisiloxane, the measured steady-state friction forces decrease: at 0.5 wt % of Octamethyltrisiloxane 54 ± 6 µN, at 1 wt % of Octamethyltrisiloxane 42 ± 9 µN and at the highest amount of Octamethyltrisiloxane used 1.5 wt % 40 ± 5 µN.

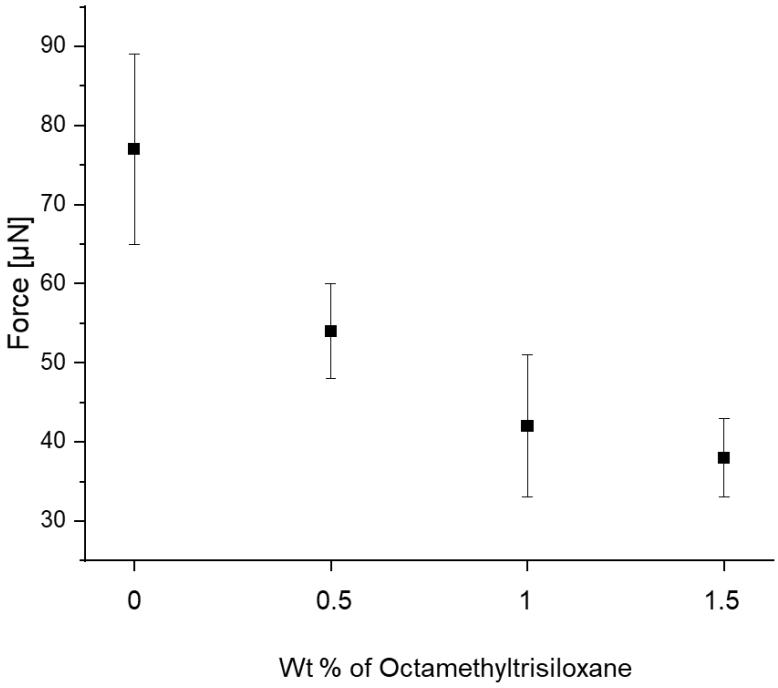

Figure 20: Average steady-state friction force with a standard deviation for four elastic PDMS surfaces (10:1) (ratio of base to crosslinker) with different wt % of Octamethyltrisiloxane in comparison to the base. The x-axis shows wt % of Octamethyltrisiloxane, the y-axis the force in µN.

The steady-state friction force could be measured on all elastic PDMS surfaces. However, a clear difference can be observed due to the addition of Octamethyltrisiloxane. In contrast, the difference in the steady-state friction force compared to the wt % of Octamethyltrisiloxane added is quite small. As presented in 4.2.2 the addition of Octamethyltrisiloxane softens a surface, since the oligomer chains are loosely attached between the polymer chains. In connection with the results from Figure 20, it is concluded that the steady-state friction force decreases with the addition of Octamethyltrisiloxane when the surface is more deformable.

The standard deviation shown in Figure 20 is justified by the uncertainty of the measurement e.g. the distance between the surface and the blade and the experimental performance. For better comparability, a higher number of runs (>5 runs) per surface should be performed.

Since the force measurement in the addition of Octamethyltrisiloxane was possible in contrast to the experiment with different crosslinker shares (see 4.2.1), the formation of the wetting ridge could have two reasons: The accumulation of shorter oligomer chains could lead to less strong interaction in the wetting ridge. Thus, less force could be needed to move the droplet. A reversible change of the surface tension by Octamethyltrisiloxane, e.g. a reduction of the surface tension, would also be hypothesized.

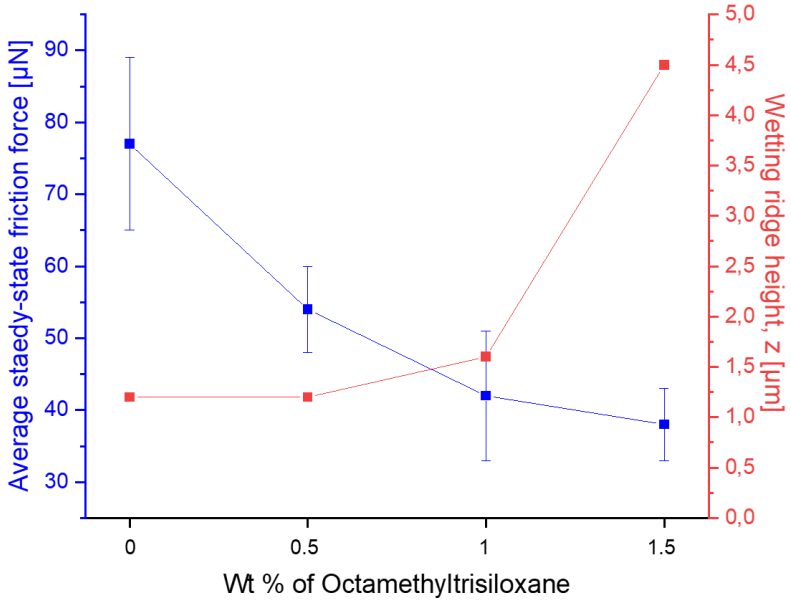

Figure 21: Average steady-state friction force with standard deviation (blue line), wetting ridge heights (red line) for the four elastic PDMS surfaces (10:1) (ratio of base to crosslinker) with different wt % of Octamethyltrisiloxane in comparison to the base. The x-axis shows the wt % of Octamethyltrisiloxane, the y-axis the force in µN. High wt% of Octamethyltrisiloxane results in lower average steady-state friction forces and larger wetting ridge height.

As a summary for this section, it is concluded that the addition of Octamethyltrisiloxane results in a variation of the steady-state friction forces and the evolution of the wetting ridges. The addition of high wt % of Octamethyltrisiloxane leads to a visible wetting ridge and low steady-state friction force between the PDMS surface and the droplet (see Figure 21). Low amounts of free oligomer chains lead to higher forces, which means that lower forces lead to a stronger interaction between droplets and the PDMS surface. Also, the average steady-state friction force values of the addition of 1 wt % and 1.5 wt % of Octamethyltrisiloxane are similar, the height of the wetting ridges is different. The evolution of such a wetting ridge as a function of the addition of Octamethyltrisiloxane might result in the greater network deformation of the elastic

PDMS surface with increasing wt % of Octamethyltrisiloxane. It is presumed, that the free oligomer chains accumulate at the three-phase contact line, resulting in the shape and size of the wetting ridge.

Wetting ridges can be analyzed both when the crosslinker share is changed and when Octamethyltrisiloxane is added. However, steady-state friction force measurement is only possible with the highest crosslinker fraction. The addition of Octamethyltrisiloxane leads to lower forces. It can be assumed that this is due to the composition of the wetting ridge or the reduction of the surface tension by Octamethyltrisiloxane.

There are still many unanswered questions about steady-state friction force measurements on these elastic PDMS surfaces. For future investigation, attention should be drawn to finding a method to measure the steady-state friction force on more elastic PDMS surfaces. A reduction of the droplet volume and the speed, as well as an increase in the surface tension of the droplet liquid, could lead to new findings.

Further research should be undertaken to investigate the influence of oligomers like Octamethyltrisiloxane with higher viscosity and the chemical composition of the surface on which the droplet no longer slides. As described in 2.4.2, the molecular weight affects the distance between the crosslinks. Using oligomers with higher viscosity increases the molecular weight, suggesting that this leads to a higher shape and size of wetting ridges. Longer oligomer chains should result in stronger interaction in the wetting ridge in comparison to shorter oligomer chains and higher steady-state friction forces.

4.3 Chemical effects

The chemical influence on elastic PDMS surfaces was analyzed based on the chemicals opened in different years in the laboratory and the humid ambient around the elastic PDMS surfaces. The results of these experiments are presented in terms of average steady-state friction force.
As seen in Figure 17 a wetting ridge on a surface with a ratio of 10:1 (base to crosslinker) could not be observed with the used objective. Therefore in this section, no wetting ridge analyses are shown.

4.3.1 Different batches of chemicals

All elastic PDMS surfaces in this section were synthesized with a ratio of 10:1 of the base to crosslinker as listed in Table 5. From Figure 22 it can be seen that elastic PDMS surfaces, synthesized by batches opened in different years show dissimilar average steady-state friction force values (see raw data in Appendix Figure 32). The

term ‘batch’ defines the elastomer kit opened in a certain year, batch 2016 was opened in 2016. The highest value around 83 ± 13 µN was found on the surface with batch 2021, the lowest value represents the oldest batch from 2016 around 54 ± 8 µN. What stands out in this figure is the steady decline of the average steady-state friction force values with batches opened in different years.

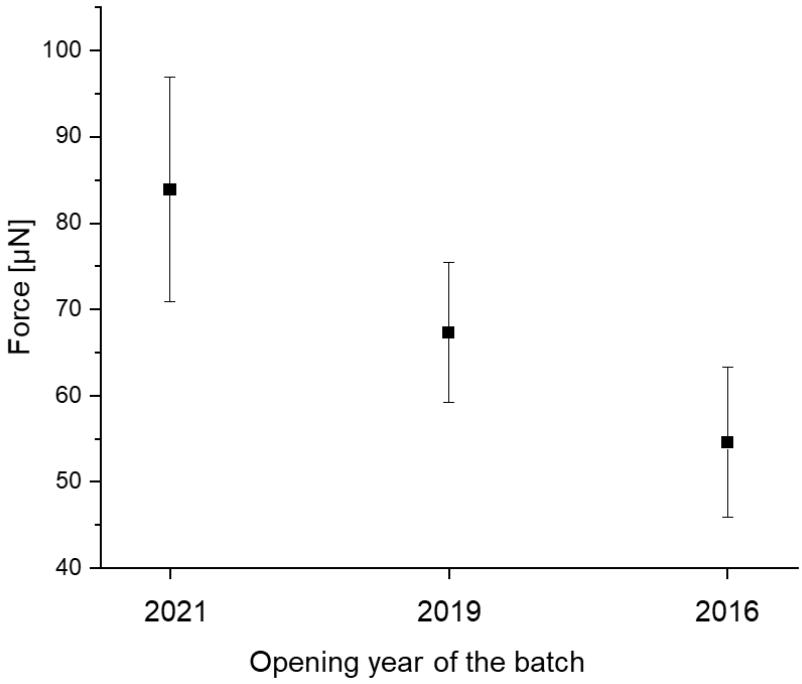

Figure 22: Average steady-state friction force with a standard deviation of three surfaces of the same elastomer kit, called a batch. The x-axis shows the opening year of the batch for the surface, the y-axis the force in µN.

These results confirm a correlation between the measured average steady-state friction force values and the opening year of the chemicals. The observed decrease in the steady-state friction force could be attributed to chemical reactions between the environment e.g. the water and either the crosslinker or the base. The results of these comparative experiments will be presented in the next sections.

4.3.2 Analyses of crosslinkers

To study the influence of the crosslinkers opened in different years on the steady-state friction force a friction experiment with these crosslinkers and the base from batch 2021 was done. Furthermore, the molecular weight distribution and silicone hydride reactivity of the crosslinker batches are presented.

4.3.2.1 Influence on the steady-state friction force

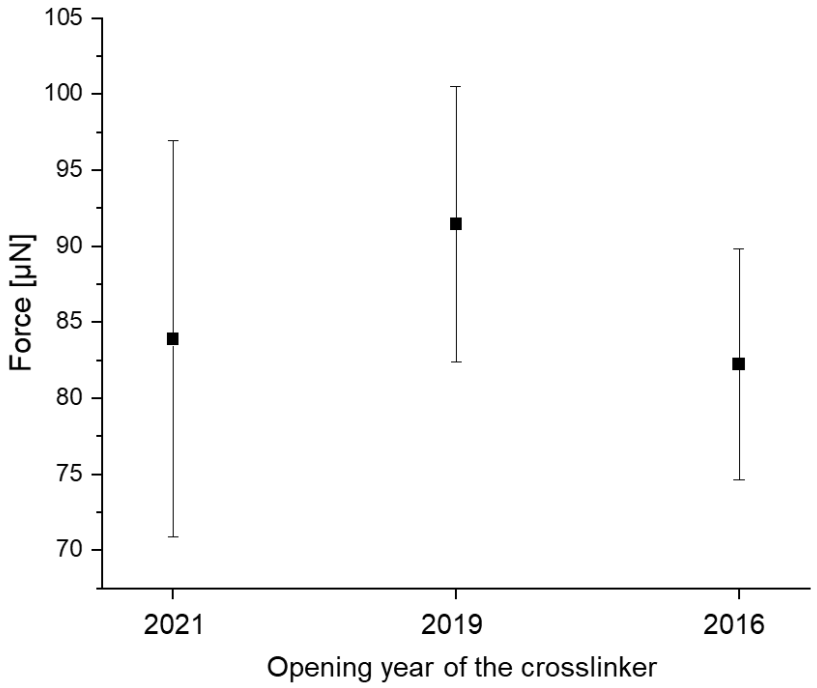

Figure 23: Average steady-state friction force with a standard deviation for three samples synthesized with the crosslinkers opened in different years. The x-axis shows the opening year of the crosslinker, the y-axis the force in µN. The base from 2021 was used for each sample.

As can be seen in Figure 23 the samples with crosslinkers opened in different years indicate comparable average steady-state friction force values. Considering the standard deviation, all average steady-state friction force values fall in the same range between 70 µN and 100 µN. The value of the sample with the crosslinker of 2019 has the highest value around 91 ± 9 µN.

These results support the idea of the same chemical composition of the synthesized elastic PDMS surfaces because there is nearly no difference between the crosslinkers opened in different years. The next section was concerned with detailed analyses of the molecular structure and the reactivity to validate the results.

4.3.2.2 Influence of the molecular weight

According to Figure 24, the crosslinkers opened in different years show two significant peaks. The first peak shows a peak maximum at a molecular weight of $2 \cdot 10^3$ g/mol and a normalized intensity of 1, whereas the second peak has a normalized intensity of 0.3 at a molecular weight of $6 \cdot 10^4$ g/mol. The functional groups of the peaks cannot

be further identified due to the unknown synthesis and exact chemical composition of the crosslinker. All crosslinker batches support the same molecular weight distribution.

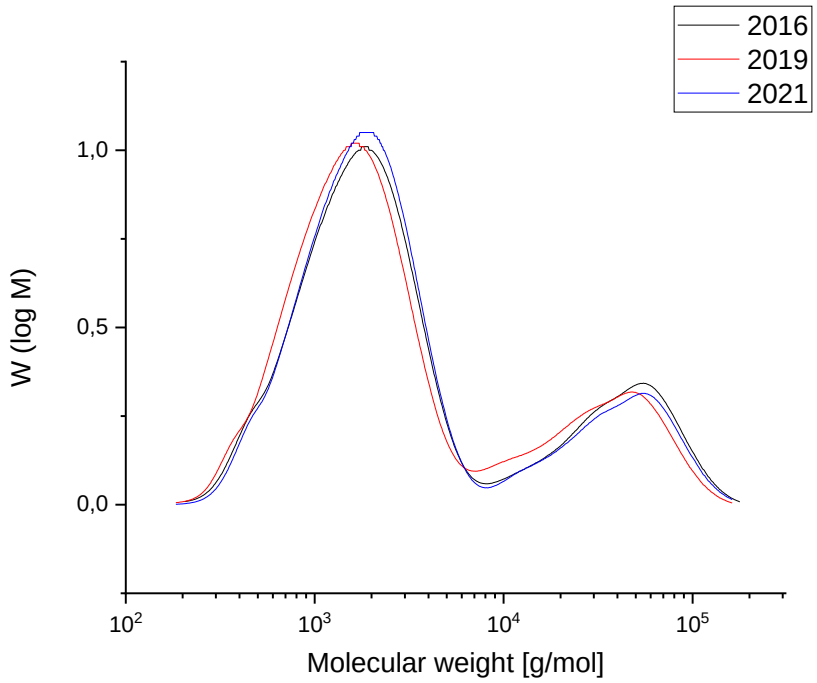

Figure 24: GPC spectrum with a molecular weight distribution for the three crosslinkers opened in different years: 2016 is shown in black, 2019 in red, and 2021 in blue. The x-axis shows the logarithmic molecular weight, the y-axis molecular weight in g/mol.

Within the range of measurement errors, there is no significant difference in molar masses and molecular mass distribution of the samples.

This result is consistent with the result of the force measurement shown before (see Figure 23).

4.3.2.3 Influence of the silicone hydride reactivity

The comparison of the intensities was done to determine the reactivity of the hydride group, which is important for the described reaction**.** The intensities of each peak refer to the number of functional groups in the analyzed crosslinker, which could react in the described reaction. The methyl groups (see Figure 25b)) show in all batches a shift of around 0.70 ppm and an intensity of 93.80. The Hydride-group represents in all batches a shift of 5.36 ppm. The intensities show only minor differences between the batches. The crosslinker of 2021 has an integral of 5.66 ppm, which is lower than the intensity of the crosslinkers from the batches 2016 and 2019 (5.89). The small peak

with a shift of 6.53 ppm is in all batches visible, it might be a Methyl (vinyl)-silane group, which comes from dimethyl vinylterminated Dimethylsiloxane, and Tetramethyl tetravinyl cyclotetrasiloxane, as described in 2.4.1.

From Figure 25b) it is observed that the peaks of the functional groups of all crosslinker batches have nearly the same shift and practically the same intensity (see Table 7).

a)

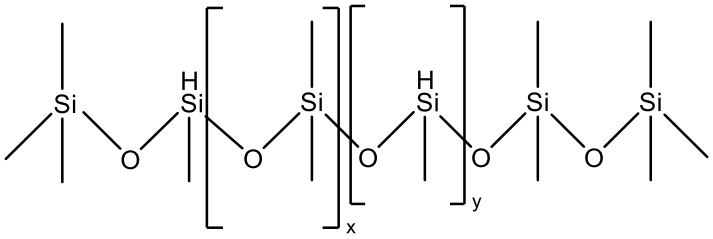

b)

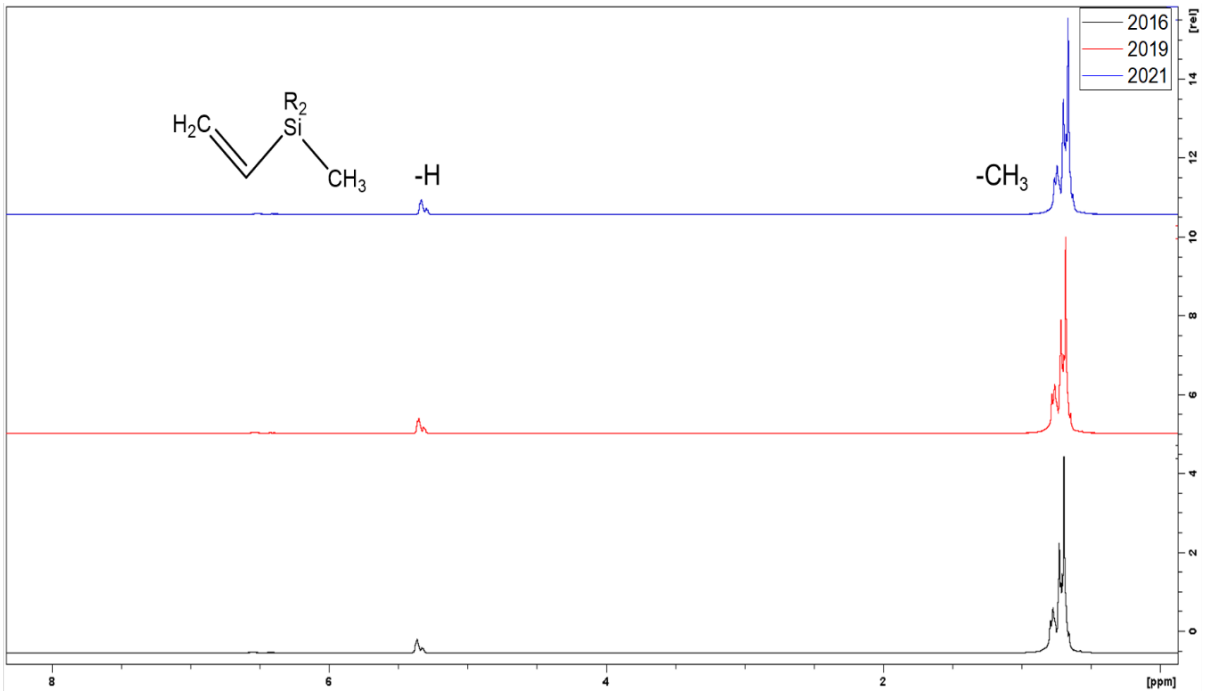

Figure 25: a) chemical structure of methyl-hydro siloxane-dimethylsiloxane, which should be the main chemical of the crosslinker[21]; b) ^{1}H-NMR spectra of the three crosslinkers opened in different years: 2016 is shown in black, 2019 in red, and 2021 in blue. The x-axis shows the shift of the functional groups in ppm, the y-axis the relative intensity.

Table 7: Shifts and Intensity of functional groups from the crosslinkers opened in different years from the ^{1}H-NMR spectra (see Figure 25).

	Crosslinker 2016		**Crosslinker 2019**		**Crosslinker 2021**	
	Shift [ppm]	Intensity	Shift [ppm]	Intensity	Shift [ppm]	Intensity
CH_2=CH-SiR_2-CH_3	6.53	1.38	6.50	1.31	6.53	1.33
-H	5.36	5.89	5.36	5.89	5.36	5.66
-CH_3	0.71	92.76	0.71	92.80	0.69	93.01

The results of the NMR analysis show no significant differences in the chemical composition of crosslinkers opened in different years. Therefore the chemical composition of the elastic PDMS surfaces should be all the same, with similar results to the force measurements.

To summarize this section no difference between surfaces synthesized with crosslinkers opened in different years was observed: Neither in the steady-state friction force measurements, nor the molecular weight (via GPC analysis), nor the reactivity of the hydride (via NMR study) and the chemical structure of the molecule.

Moreover, the force difference between the batches seen in Figure 22 is not affected by the crosslinker.

4.3.3 Analyses of bases

To investigate the influence of the base on the steady-state friction force, a friction experiment was performed comparing the bases opened in different years with the crosslinker, which was opened in 2021. Furthermore, the molecular weight distribution analysis and vinyl group reactivity study on the base batches are presented.

4.3.3.1 Influence on the steady-state friction force

Figure 26 demonstrates the effect on the average steady-state friction force of the bases opened in different years with the crosslinker from 2021 in all samples. The highest average steady-state friction force value shows the batch from 2021 around 83 ± 13 µN. The average values of the bases opened 2019 (61 ± 7 µN) and 2016 (58 ± 6 µN) are significantly lower than the batch 2021.

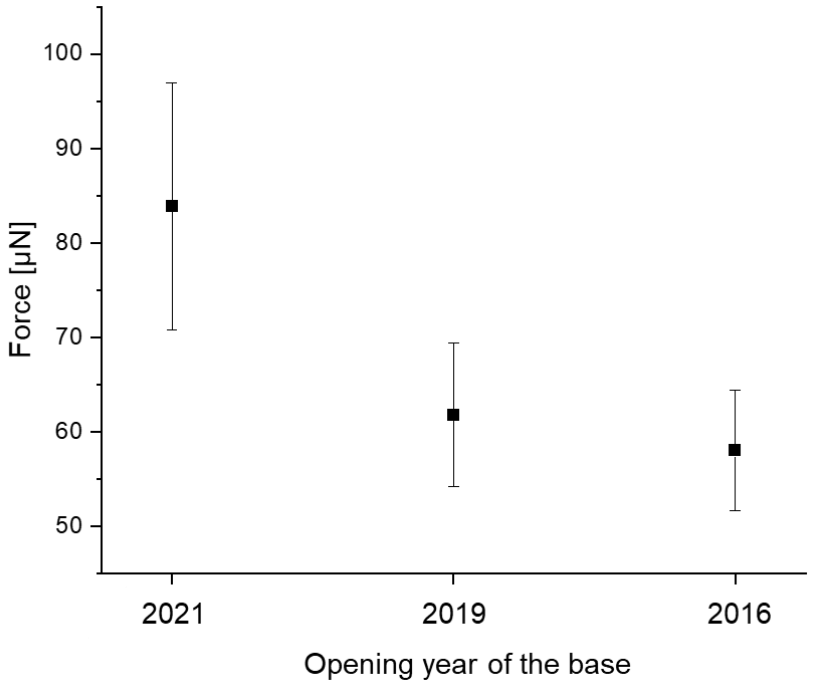

Figure 26: Average steady-state friction force with a standard deviation for three samples with the bases opened in different years. The x-axis shows the opening year of the base, the y-axis the force in µN. The crosslinker from 2021 was used for each sample.

During the friction force measurements, no difference in the behavior of the droplet could be detected, e.g. when the droplet slips under the blade.

A possible explanation for these results might be a chemical reaction with the base during storage in the laboratory. In Figure 27a) the bases opened in different years could react with the water in the ambient air. The polymer chain of the base would break into two smaller polymer fractions, whereas in Figure 27b) a product from a) could react with a base molecule through opening a double bond, which leads to a longer molecule. As a result of this possible reaction, the molecular weight would be changed. In order to verify these considerations, a GPC spectrum for the molecular weight and a ^{1}H-NMR spectrum for the vinyl group reactivity are presented.

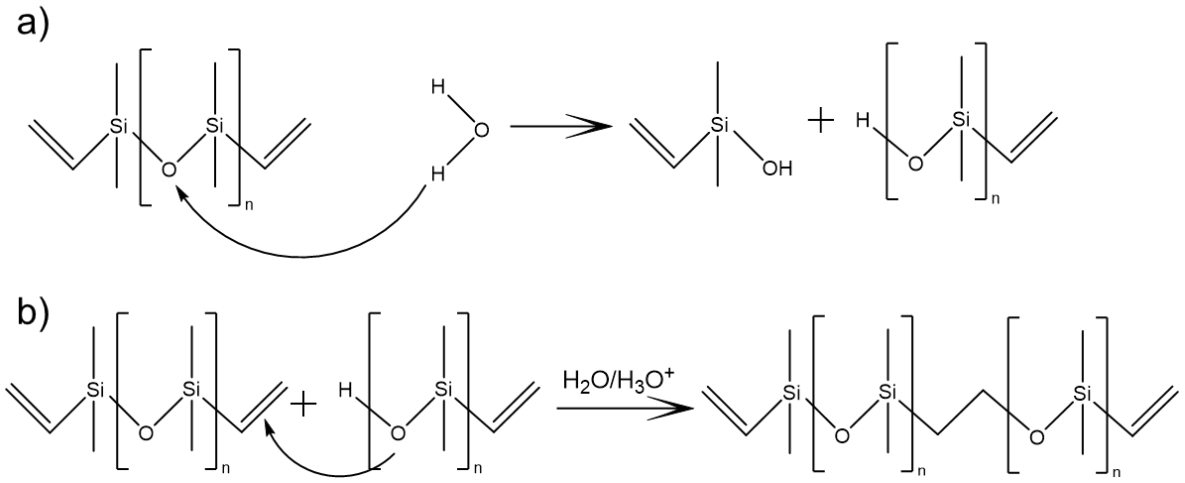

Figure 27: Potential reaction of the bases opened in different years with the water in the air ambient. In a) The fracture of the polymer chains in two smaller fractions is shown, whereas in b) a product from a) could react with a base molecule through opening a double bond.

4.3.3.2 Influence of the molecular weight

According to Figure 28, the different bases opened in different years show one significant peak and one shoulder. The peak shows a peak maximum at a molecular weight of $5 \cdot 10^4$ g/mol and a normalized intensity of 1. All base batches support the same molecular weight distribution.

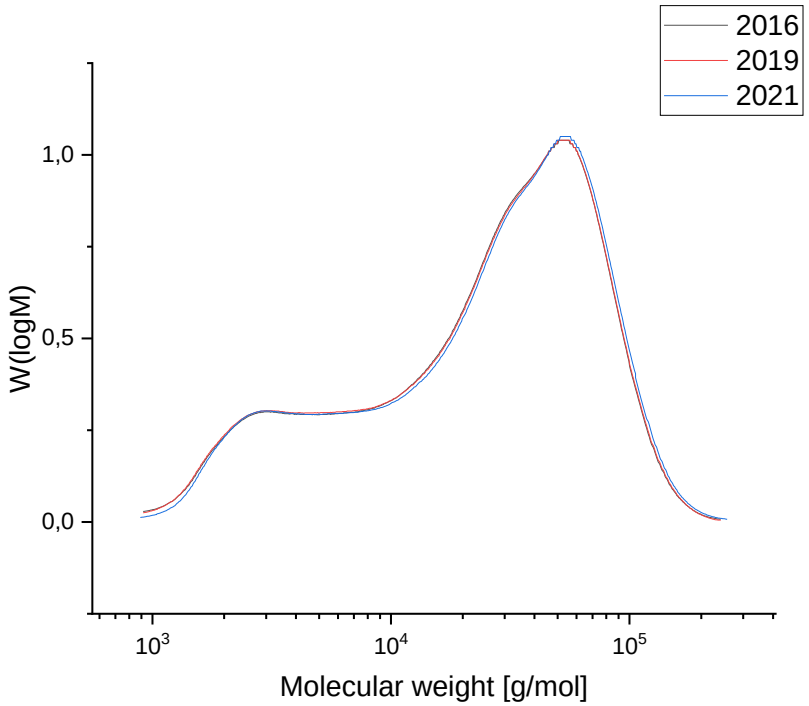

Figure 28: GPC spectrum with a molecular weight distribution for the three bases opened in different years: 2016 is shown in black, 2019 in red, and 2021 in blue. The x-axis shows the logarithmic molecular weight, the y-axis molecular weight in g/mol.

Within the range of measurement errors, there is no significant difference in molar masses and molecular mass distribution of the samples.

With this result, the reason for the steady-state friction force distinctions is not reflected in the molecular weight distribution. Chemical reactions with the water in the air would change the molecular weight, which is with this result not explainable anymore.

4.3.3.3 Influence of the vinyl group reactivity

The ^{1}H-NMR spectra of the bases opened in different years are shown in Figure 29b) and c). It is observed that the peaks of the functional groups of all base batches have nearly the same shift and practically the same intensity (see Table 8). The intensities of each peak refer to the number of functional groups in the analyzed chemical, which could react in the described reaction.

a)

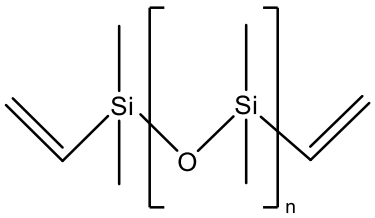

b)

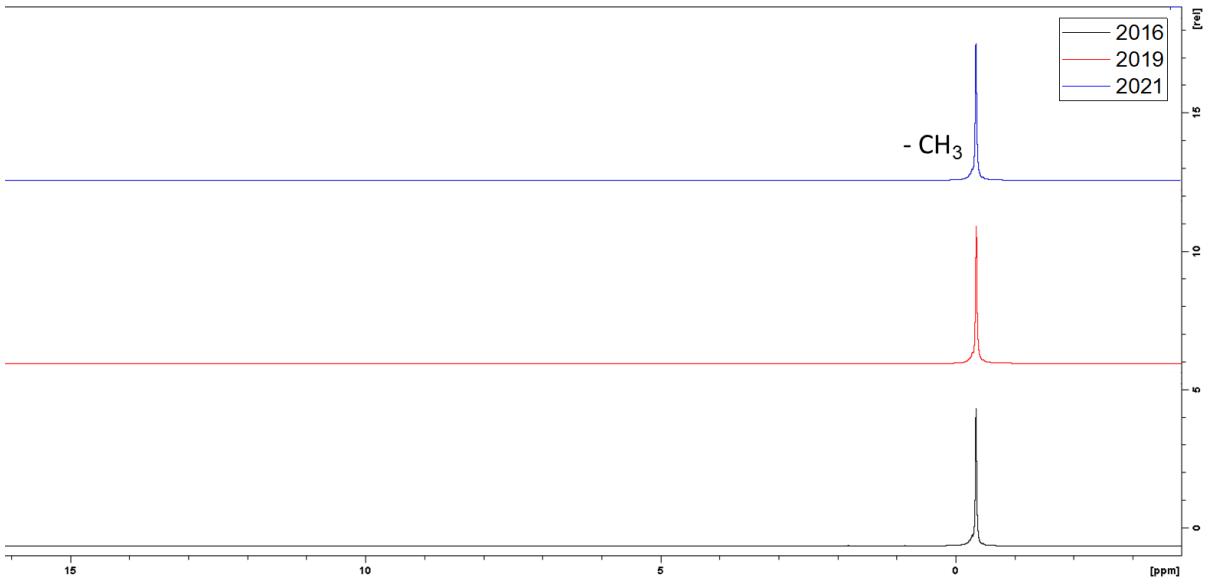

c)

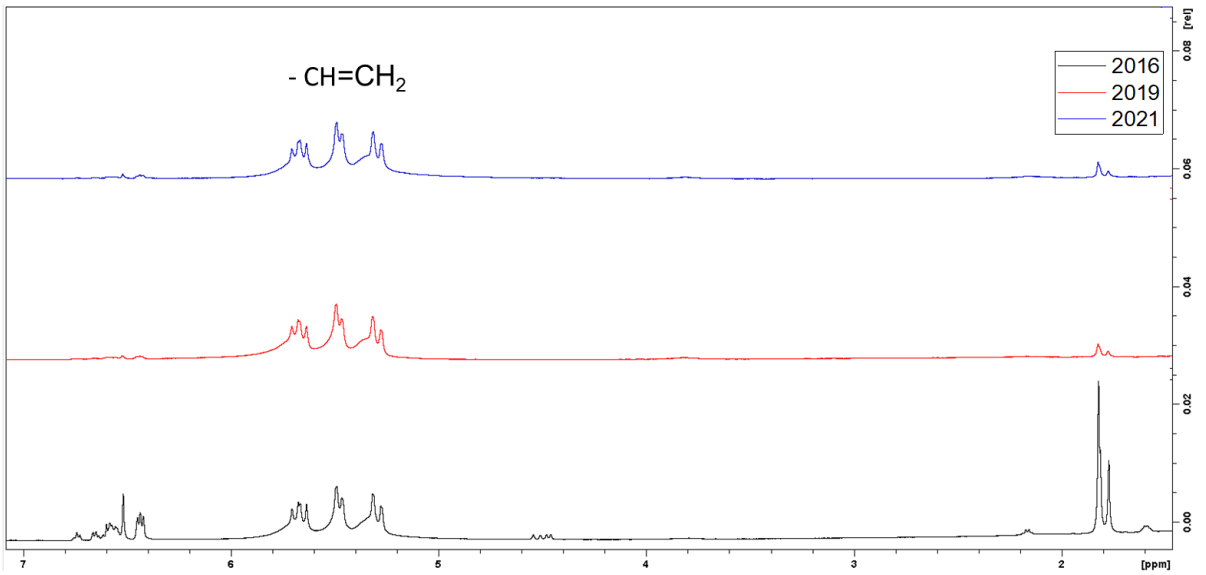

Figure 29: a) chemical structure of vinyl-terminated PDMS, which should be the main chemical of the crosslinker[21]; b) ^{1}H-NMR spectra of the three bases opened in different years: 2016 is shown in black, 2019 in red, and 2021 in blue; c) Zoom in between 2,5 ppm and 7 ppm. The x-axis shows the shift of the functional groups in ppm, the y-axis the relative intensity.

In all three batches the methyl groups are depicted at a shift of –0.32 ppm with an intensity of 98.87 ppm (see Figure 29b)). In the zoomed spectra (Figure 29c)) the peak at a shift of 5.50 ppm with an intensity of 0.93 is seen, which is the vinyl group. The comparison of the intensities was done to determine the reactivity of the vinyl group, which is important for the described reaction**.** An interesting finding is a low-molecular vinyl structure at a shift of 6.5 ppm and a peak at 1.8 ppm in the spectra of the base opened in 2016.

Table 8: Shifts and Intensity of functional groups from the bases opened in different years from the ^{1}H-NMR spectra (see Figure 29).

	Base 2016		**Base 2019**		**Base 2021**	
	Shift [ppm]	Intensity	Shift [ppm]	Intensity	Shift [ppm]	Intensity
-CH=CH$_2$	5.51	0,92	5.49	0,93	5,50	0,93
-CH$_3$	-0,32	98,87	-0,31	98,98	-0,32	98,76

The results of the NMR analysis show no significant differences in the analyzed bases opened in different years in the ratio of methyl to vinyl groups. As this ratio is identical, the chemical composition of the elastic PDMS surfaces should be all the same, with similar results to the force measurements.

In conclusion for this section, the results of experiments done with the bases opened in different years reveal differences due to the steady-state friction force, also all batches depict the same molecular weight distribution. The possible reaction shown in Figure 27 is not reasonable anymore due to all batches showing the same reactivity. It might be that the base opened in 2016 contains more vinyl groups due to contamination, which would lead to more free chains and lower steady-state friction forces. However, this does not explain the decrease in the steady-state friction force from the base opened in 2019. The ^{1}H-NMR spectra depict the same reactivity in the vinyl bond in all base batches, also the base opened in 2016 is a low-molecular substance, which could not be identified in detail.

4.3.4 Influence of the humidity

To analyze the influence of humidity, samples with a composition of 10:1 (base to crosslinker) were kept in 2 desiccators under different conditions over 3 weeks. One desiccator had low humidity (around 5 %) and the other had high humidity (around 64 %). Within 3 weeks, four attempts were made to measure the force. It was not possible to measure the force. The droplet hit the blade, detached from the blade

again, and remained on the surface, as described in 4.2.1.2. The results are equivalent to the curves described in Figure 18. A steady-state friction force (described in 4.1.2) could not be determined. It was not possible to determine a wetting ridge due to using no fluorescent dyes. Also, for the surface samples, which were stored for three weeks at room temperature under air conditions it was not possible to measure the forces.

4.3.5 Conclusion

In this section, the results of chemical influences were presented. The results of steady-state friction forces of base/crosslinkers opened in different years are summarized in Figure 30. Samples that contain a base and/or crosslinker opened in 2019 are marked in red, the black samples consist of a base and/or crosslinker opened in 2016 in different combinations. The average steady-state friction force values of the samples containing base or crosslinker opened in 2019 are consistently higher than the samples containing base or crosslinker opened in 2016. The highest average steady-state friction force values give the samples consisting of the base opened in 2021 and the crosslinkers opened in 2019 and 2016. The average steady-state friction force of both batches is around 91 ± 9 µN (2019) and 82 ± 7 µN (2016). The pure batches (base and crosslinker from the same batch) provide average steady-state friction force values around 67 ± 8 µN (2019) and 54 ± 8 µN (2016), using the crosslinker from batch 2021 the average steady-state friction force values are similar to the pure batches: 61 ± 7 µN (base opened 2019) and 58 ± 6 µN (base opened 2016).

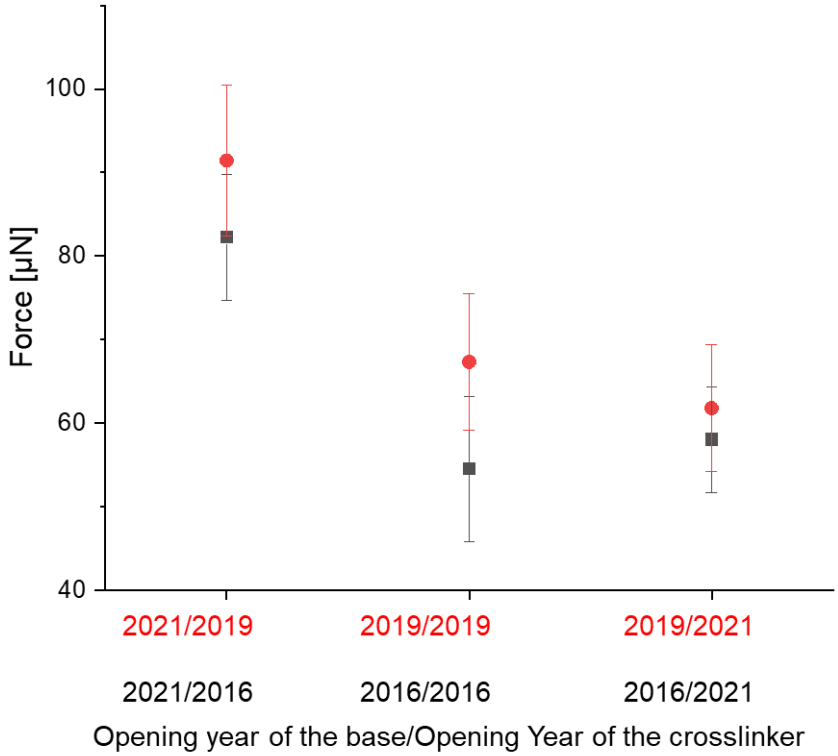

Figure 30: Average steady-state friction force with a standard deviation for three samples each with the base/crosslinker opened in 2019 (red) and 2016 (black). The x-axis shows the opening year of the chemicals in the order of Base/Crosslinker, the y-axis the force in µN.

The results indicate that the effect of the crosslinker is significantly lower than the effect of the base.

An explanation for the differences in the steady-state friction forces was not identified. It might be bulk effects, which could not be detected by the analyses of the educts. Further analyses with bulk active methods such as energy-dispersive X-ray spectroscopy (EDX) or rheological investigations are necessary for clarification.

It was not possible to clarify the effect of the humidity of elastic PDMS surfaces, as the droplets remained on the surface. With these results, it validates for this reaction at higher temperatures than room temperature for the crosslinking process. Further research should be done for analyzing the humidity effect for a longer time range to facilitate the crosslinking process at room temperature done 21 days for this thesis.

5 Conclusions and Outlook

The purpose of the current thesis was to determine the physical (variation of crosslinker ratio and addition of Octamethyltrisiloxane as an oligomer) and the chemical influence (based on the chemicals opened in different years in the laboratory) on the steady-state friction force between a droplet and a PDMS surface during droplet sliding and the evolution of wetting ridges. Wetting ridges were recorded by optical visualization with LSCM and the steady-state friction force was measured with a sensory setup.

The investigation of the physical effects has shown that the friction by variation of the crosslinker share could not be quantified with the used setup. Just for the surface with a ratio of 10:1 (base to crosslinker) a steady-state friction force could be measured. For all other surfaces with a lower share of a crosslinker (e.g. 60:1), it was not possible to measure the forces due to strong interactions between the elastic PDMS surface and the droplet. This can be seen in the evolution of the wetting ridge.

The additional amount of Octamethyltrisiloxane as an oligomer made a small difference in the steady-state friction force results. But the evolution of the wetting ridges is visible the more Octamethyltrisiloxane was added. It was shown, that the addition of Octamethyltrisiloxane leads to lower forces. It can be assumed that this is due to the changed composition of the wetting ridge or the reduction of the surface tension by Octamethyltrisiloxane.

The major finding of the analyses of the chemical effects was the difference in the steady-state friction force values between the batches opened in different years.

Analyses of the crosslinkers opened in different years were done by steady-state friction force measurements, GPC, and NMR. All analyses revealed similar results in the steady-state friction force, molecular weight, and the reactivity of the specific functional group (hydride group).

Analyses of the bases opened in different years provide various results of the average steady-state friction force, while the molecular weight is identical. As the ratio of methyl to vinyl groups is in all batches identical, the chemical composition of the elastic PDMS surfaces should be all the same, with similar results to the force measurements. Although in base opened in 2016 exists some low molecular vinyl groups.

The investigation of the humidity experiment has demonstrated that a higher temperature than room temperature is necessary for the crosslinking process.

A more systematic approach for new insights into the evolution of wetting ridges would be an oil immersion objective matched to the refractive index of the used PDMS.

The question raised is the investigation of a measurement method for steady-state friction forces on elastic PDMS surfaces with chemical compositions like 60:1 (ratio of base to crosslinker). Different parameters can reduce the adhesion force of the droplet, such as volume, speed, and surface tension. A smaller volume leads to a decreased

deformation of the PDMS surface, which leads to lower forces. Alternatively, with less speed, the applied force should have it easier to move the wetting ridge on the PDMS surface.

Further research should be undertaken to investigate the influence of oligomers like Octamethyltrisiloxane with higher viscosity. Additionally, the chemical composition of the PDMS surface on which the droplet no longer slides should be analyzed. Using oligomers with higher viscosity increases the molecular weight, suggesting that this leads to a higher shape and size of wetting ridges. Longer oligomer chains should result in stronger interaction in the wetting ridge in comparison to shorter oligomer chains and higher steady-state friction forces.

Further research should be done for analyzing the humidity effect for a longer time range to facilitate the crosslinking process at room temperature. In addition, the evolution of wetting ridges with Lumogen dyed elastic PDMS surfaces under different humid conditions should also be investigated.

More information on the chemical composition of the applied base and crosslinker would help to establish more insights into the reaction. This could give comparisons with ^{1}H-NMR analyses with pure chemicals, which are found in the base and crosslinker. An approach to tackle this issue could be to mix the pure chemicals in the laboratory and to vary the components and the catalyst. The low molecular vinyl groups found in the base opened in 2016 which need to be identified in detail in further research with diffusion ordered spectroscopy (DOSY).

In future, care should be taken to the effect of the curing temperature. It would be beneficial to have the same curing temperature surface preparation for the steady-state friction force measurements (used temperature: 60 °C) and the visualization of the wetting ridges (used temperature: 40 °C). A starting point should be the analyses of the steady-state friction forces and the wetting ridges of the elastic PDMS surfaces cured at 40 °C and 60 °C.

Better reproducibility of the force measurements should be explored, by analyzing the distance between the surface and the blade. A higher reproducibility would be gained by using in each measurement the same position of the droplet, where the blade reaches the droplet first. Further research might explore the influence of the stiffness of the used metal blade for the steady-state friction force measurements. In future, the experimental investigations should also consider the droplet deformation and the droplet width for the calculation of the forces.

The functionalization of the blade should be validated and the dependency between, the droplet sliding under the blade, and the functionalization of the blade investigated. Further research might explore the behavior of the droplet with differently functionalized blades (hydrophilic/hydrophobic). A separate functionalization holds promise to make the lowest blade part hydrophilic and the remaining part hydrophobic.

In general, it would be recommended to use new mixed chemicals e.g. the dissolved Atto 488 in glycerol/water. It is assumed, that the mixture changed in concentration and chemical composition, over the years, due to evaporation, which could lead to a change in the surface tension.

The static measurement of wetting ridges is a well reproducible and stable method to gain insights into the interactions between PDMS surface and droplet. Further research is needed to understand the size and shape of wetting ridges e.g. by using different fluorescent dyes between polymer networks and loosely arranged oligomers. Research is also needed to find a method for measuring the wetting ridge in dynamic mode.

The measurement would be much easier if the friction force and the wetting ridge could be analyzed simultaneously.

Research is also needed to determine the effect of the steady-state friction force, and the wetting ridge of the sample storage under air and nitrogen.

Further research could usefully explore the bulk effects of elastic PDMS surfaces with techniques like energy-dispersive X-ray spectroscopy (EDX) or rheological investigations.

More insights into dissipation mechanisms on elastic PDMS surfaces would be gained with additional measurement of the shear and storage modulus by shear rheology.

The applied method for measuring steady-state friction forces, while sliding droplets over the surface, is a new approach and a promising method for characterizing elastomers. Further experimental research should be carried out to establish the method for more elastic surfaces.

This thesis shows that the ratio of crosslinker and the addition of Octamethyltrisiloxane change the polymeric network, which is seen in the steady-state friction force measurements and the evolution of wetting ridges. These findings suggest that the bacterial contamination (as described in 1) changes with different chemical compositions of the PDMS surface. Further studies regarding the role of elastic PDMS surfaces on bacterial contamination would be worthwhile.

6 Appendix

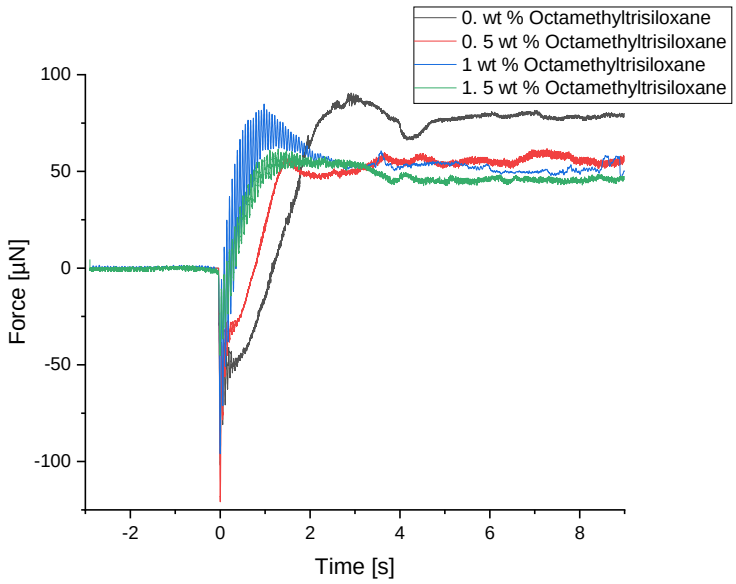

Figure 31: Raw data of the force curve on a PDMS surface (10:1) (ratio of base to crosslinker) with different wt % of Octamethyltrisiloxane in comparison to the base. The x-axis shows the chemical composition of the surface, the y-axis the force in µN. The surface without the addition of Octamethyltrisiloxane shows the grey line, the surface with the addition of 0.5 wt % of Octamethyltrisiloxane shows the red line, the surface with the addition of 1 wt % of Octamethyltrisiloxane shows the blue line, the surface with the highest addition of Octamethyltrisiloxane (1.5 wt%) shows the green line.

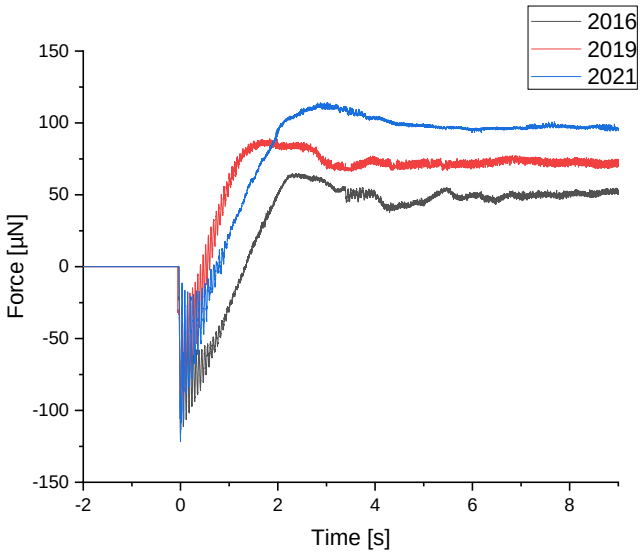

Figure 32: Raw data of the force curves on a PDMS surface (10:1) (ratio of base to crosslinker) with batches opened in different years: in black the batch opened in 2016, in red the batch opened in 2019, and in blue the batch opened in 2021. The x-axis shows the time in s, the y-axis the force in µN.

7 List of references

1. Bartalena, G., Loosli, Y., Zambelli, T. & Snedeker, J. G. Biomaterial surface modifications can dominate cell-substrate mechanics: The impact of PDMS plasma treatment on a quantitative assay of cell stiffness. *Soft Matter* **8**, 673–681 (2012).

2. Kim, Y. D., Dordick, J. S. & Clark, D. S. Siloxane-based biocatalytic films and paints for use as reactive coatings. *Biotechnol. Bioeng.* **72**, 475–482 (2001).

3. Ammar, S., Ramesh, K., Vengadaesvaran, B., Ramesh, S. & Arof, A. K. Amelioration of anticorrosion and hydrophobic properties of epoxy/PDMS composite coatings containing nano ZnO particles. *Prog. Org. Coatings* **92**, 54–65 (2016).

4. Xu, S. *et al.* Soft microfluidic assemblies of sensors, circuits, and radios for the skin. *Science (80-.).* **344**, 70–74 (2014).

5. Srisa-Art, M.; Noblitt, S.D.; Krummel, A.T.; Henry, C. . IR-Compatible PDMS microfluidic devices for monitoring of enzyme kinetics. 2018, 1021, 95–102. *Anal. Chim. Acta* 95–102 (2018).

6. Lavielle, N., Asker, D. & Hatton, B. D. Lubrication dynamics of swollen silicones to limit long term fouling and microbial biofilms. *Soft Matter* **17**, 936–946 (2021).

7. Armugam, A. *et al.* Broad spectrum antimicrobial PDMS-based biomaterial for catheter fabrication. *Biomater. Res.* **25**, 1–13 (2021).

8. Snowden, J. N., Beaver, M., Smeltzer, M. S. & Kielian, T. Biofilm-infected intracerebroventricular shunts elicit inflammation within the central nervous system. *Infect. Immun.* **80**, 3206–3214 (2012).

9. G. M., K. *et al.* Antimicrobial resistance and COVID-19: Intersections and implications. *Elife* **10**, e64139 (2021).

10. Tunkel, A. R. *et al.* Practice guidelines for the management of bacterial meningitis. *Clin. Infect. Dis.* **39**, 1267–1284 (2004).

11. Cai, Z., Skabeev, A., Morozova, S. & Pham, J. T. Fluid separation and network deformation in wetting of soft and swollen surfaces. *Commun. Mater.* **2**, (2021).

12. Naga, A. *et al.* How a water drop removes a particle from a hydrophobic surface. *Soft Matter* **17**, 1746–1755 (2021).

13. Butt, H., Graf, K. & Kappl, M. *Physics and Chemistry of Interfaces*. *Physics and Chemistry of Interfaces* (2003). doi:10.1002/3527602313.

14. Bico, J., Reyssat, É. & Roman, B. Elastocapillarity: When Surface Tension Deforms Elastic Solids. *Annu. Rev. Fluid Mech.* **50**, 629–659 (2018).

15. Young, T. An essay on cohesion of fluides. *Philos. Trans R. Soc.* **95**, 65–87 (1805).

16. Good, R. T. Contact angle, wetting, and adhesion: a critical review. *J. Adhes. Sci. Technol.* **6**, 1269–1302 (1992).

17. Pilat, D. W. *et al.* Dynamic measurement of the force required to move a liquid drop on a solid surface. *Langmuir* **28**, 16812–16820 (2012).

18. Gao, N. *et al.* How drops start sliding over solid surfaces. *Nat. Phys.* **14**, 191–196 (2018).

19. Hooke, R. De Potentia Restitutiva, or of Spring. Explaining the Power of Springing Bodies. (1678).

20. Campbell, D. J. *et al.* Replication and Compression of Bulk and Surface Structures with

Polydimethylsiloxane Elastomer. *J. Chem. Educ.* **76**, 537–541 (1999).

21. Ortiz-Acosta, D. & Densmore, C. Title: Sylgard® Cure Inhibition Characterization Sylgard® Cure Inhibition Characterization. (2532).

22. Fragiadakis, D., Pissis, P. & Bokobza, L. Glass transition and molecular dynamics in poly(dimethylsiloxane)/silica nanocomposites. *Polymer (Guildf).* **46**, 6001–6008 (2005).

23. Jenkins, A. D., Stepto, R. F. T., Kratochvíl, P. & Suter, U. W. Glossary of basic terms in polymer science (IUPAC Recommendations 1996). *Pure Appl. Chem.* **68**, 2287–2311 (1996).

24. Venkatachalam, S. & Hourlier, D. Heat treatment of commercial Polydimethylsiloxane PDMS precursors: Part I. Towards conversion of patternable soft gels into hard ceramics. *Ceram. Int.* **45**, 6255–6262 (2019).

25. Moučka, R., Sedlačík, M., Osička, J. & Pata, V. Mechanical properties of bulk Sylgard 184 and its extension with silicone oil. *Sci. Rep.* **11**, 1–9 (2021).

26. Xia, Y. & Whitesides, G. M. Soft lithography. *Angew. Chemie - Int. Ed.* **37**, 550–575 (1998).

27. Nakajima, Y. & Shimada, S. Hydrosilylation Reaction of Olefins: Recent Advances and PErspective. *R. Soc. Chem. Adv. Adv.* **5**, 20603–20616 (2015).

28. Matloka, P. P., Sworen, J. C., Zuluaga, F. & Wagener, K. B. Chain-end and chain-internal crosslinking in ‘latent reactive’ silicon elastomers. *Macromol. Chem. Phys.* **206**, 218–226 (2005).

29. Esteves, A. C. C. *et al.* Influence of cross-linker concentration on the cross-linking of PDMS and the network structures formed. *Polymer (Guildf).* **50**, 3955–3966 (2009).

30. Belmonte, A., Fernández-Francos, X., Serra, À. & De la Flor, S. Phenomenological characterization of sequential dual-curing of off-stoichiometric “thiol-epoxy” systems: Towards applicability. *Mater. Des.* **113**, 116–127 (2017).

31. Claesson, H. *et al.* Semi-crystalline thermoset resins: Tailoring rheological properties in melt using comb structures with crystalline grafts. *Prog. Org. Coatings* **49**, 13–22 (2004).

32. Chalk, A. J. & Harrod, J. F. Hydrosilation of Olefins Catalyzed by. *J. Am. Chem. Soc.* **87**, 16–21 (1965).

33. Amos, W. B. & White, J. G. How the confocal laser scanning microscope entered biological research. *Biol. Cell* **95**, 335–342 (2003).

34. Mayr, T. Lumogen Red F300, retrieved March 30.2022, from http://www.fluorophores.tugraz.at/substance/748.

35. Naga, A. Capillary interactions in wetting : rotation of particles at interfaces and removal of particles by drops. Dissertation physics (2021).

36. Wong, W. S. Y. *et al.* Adaptive Wetting of Polydimethylsiloxane. *Langmuir* **36**, 7236–7245 (2020).

37. Cai, Z. & Pham, J. T. How Swelling, Cross-Linking, and Aging Affect Drop Pinning on Lubricant-Infused, Low Modulus Elastomers. *ACS Appl. Polym. Mater.* (2022) doi:10.1021/acsapm.1c01455.

Acknowledgments

First of all, I would like to thank my supervisors Doris Vollmer and Georg Schied, and my tutor Lukas Hauer. You provided me with an interesting topic – even if it turned out a little different than expected. The fruitful discussions with you as well as your helpful feedback and scientific expertise have helped to progress with the project also in challenging situations. Thank you for taking the time and being patient, even if some things took longer.

I thank all the other members of the working group ‘Physics at interfaces’ for all the help in the lab, the supportive words at the right time, and for always having an open ear and a word of support.

I would like to thank Christine Rosenauer and Manfred Wagner for measuring the GPC/NMR spectra and for the fruitful discussions. My thank goes to Anke Kaltbeitzel for the helpful discussions and writing of the ImageJ script. I thank Alexander Saal for the fruitful discussions, help, suggestions, and assistance.

Thank you, Hans-Jürgen, for giving me the opportunity to write the master thesis at MPIP and to participate with the working group ‘Physics at interfaces’ in the Group Retreat in Berlin in September 2021.

Finally, I want to express my greatest thanks to my family and my friends for their support and help in my studies.

Statement of independent work

I hereby confirm that this thesis was written independently by myself without the use of any sources beyond those cited, and all passages and ideas taken from other sources are cited accordingly.

Weisenheim am Sand, 31.03.2022 _____

(Signature)